nature communications

Article

https://doi.org/10.1038/s41467-024-54242-w

Determining the rate-limiting processes for cell division in *Escherichia coli*

Received: 1 March 2024

Accepted: 1 November 2024

Published online: 16 November 2024

Check for updates

Jaana Männik[1], Prathitha Kar[2,3], Chathuddasie Amarasinghe[1], Ariel Amir[4] & Jaan Männik[1]

A critical cell cycle checkpoint for most bacteria is the onset of constriction when the septal peptidoglycan synthesis starts. According to the current understanding, the arrival of FtsN to midcell triggers this checkpoint in *Escherichia coli*. Recent structural and in vitro data suggests that recruitment of FtsN to the Z-ring leads to a conformational switch in actin-like FtsA, which links FtsZ protofilaments to the cell membrane and acts as a hub for the late divisome proteins. Here, we investigate this putative pathway using in vivo measurements and stochastic cell cycle modeling at moderately fast growth rates. Quantitatively upregulating protein concentrations and determining the resulting division timings shows that FtsN and FtsA numbers are not rate-limiting for the division in *E. coli*. However, at higher overexpression levels, they affect divisions: FtsN by accelerating and FtsA by inhibiting them. At the same time, we find that the FtsZ numbers in the cell are one of the rate-limiting factors for cell divisions in *E. coli*. Altogether, these findings suggest that instead of FtsN, accumulation of FtsZ in the Z-ring is one of the main drivers of the onset of constriction in *E. coli* at faster growth rates.

In most known bacterial species, cell division starts with the formation of the cytokinetic ring, the Z-ring, at the cell's middle[1,2]. In *Escherichia coli*, the Z-ring consists of FtsZ protofilaments anchored to the inner membrane via FtsA and ZipA linker proteins. FtsZ protofilaments in the cytokinetic ring are dynamic, undergoing a treadmilling motion[3,4]. TEM and super-resolution imaging have shown that the Z-ring consists of a sparse set of loosely associated filaments which are distributed in a narrow band (50 nm) around the midcell[5,6]. The timing for the formation of the Z-ring depends on growth conditions starting mostly at cell birth in fast growth rates but being delayed when cells are grown in a poorer quality medium[7]. Despite the early presence of the Z-ring, the cells do not initiate the onset of constriction concurrent with the formation of the Z-ring. Instead, there is a delay that lasts about ¼ of the cell cycle in *E. coli* for a range of different growth conditions[8,9].

While the Z-ring is a prerequisite for cell division, the onset of constriction acts as an effective cell cycle checkpoint[10,11]. Despite this significance, the signal that triggers the onset of constriction in *E. coli* and other bacteria has remained undetermined. Prior to the onset of constriction, a number of essential divisome proteins are recruited to the midcell. The order of recruitment of these proteins has been determined to be FtsE-FtsX and FtsK→FtsQ-FtsB-FtsL→FtsW-FtsI→FtsN[12]. Depletion or inactivation of upstream proteins prevents the recruitment of all downstream components. FtsN is the last essential component to arrive at the divisome, and it accumulates in a self-enhancing manner. Accordingly, it has been considered the trigger protein for cell division in *E. coli*[13–21].

During the onset of constriction, a core divisome complex that includes the peptidoglycan synthesizing unit FtsWI[22] separates from the treadmilling FtsZ protofilaments[23]. It has been proposed that this separation and subsequent peptidoglycan synthesis is due to the binding of FtsN to the FtsBQL complex that, in turn, activates FtsWI[19,24]. Before separation, FtsBQL and FtsWI are either associated with stationary FtsZ monomers or follow FtsZ treadmilling protofilaments via tracking their ends[23] by the diffusion-and-capture mechanism[25].

[1]Department of Physics and Astronomy, University of Tennessee, Knoxville, TN 37996, USA. [2]John A. Paulson School of Engineering and Applied Sciences, Harvard University, Cambridge, MA 02134, USA. [3]Department of Chemistry and Chemical Biology, Harvard University, Cambridge, MA 02134, USA. [4]Department of Physics of Complex Systems, Weizmann Institute of Science, Rehovot, Israel. e-mail: JMannik@utk.edu

A different pathway to trigger the checkpoint has also been proposed, in which a change in the oligomerization state of FtsA initiates the synthesis of septal cell wall[1,26,27]. FtsA, which shares its fold with actin, forms oligomeric structures in vitro[28]. These structures include 12-mer minirings, curved arcs, and antiparallel double filaments[20,29,30]. Of these higher-order structures, the experimental evidence in vivo exists only for the FtsA antiparallel filaments[20]. It has been proposed that the onset of constriction is triggered by the transformation of FtsA minirings to antiparallel filaments[1] or, alternatively, that mostly monomeric FtsA is driven to antiparallel filament form as a result of FtsN binding[20].

While the protein-protein interactions between FtsN, FtsA, and other divisome proteins are needed to trigger the onset of constriction, it has remained unclear what causes the switching on of these interactions during the cell cycle. There is no evidence of phosphorylation nor any other post-translational or slow conformational changes of these proteins. As such, the protein-protein interactions involved remain immutable in the cell cycle. On the other hand, *E. coli* and other bacteria have been observed to add approximately a constant length increment from one DNA replication initiation to the next[31] and from birth to division, irrespective of their birth length[32,33]. The latter phenomenon, referred to as the cell size adder, can be explained if cell division is triggered when a number of some protein in the cell reaches a threshold value[31,34,35]. Most different protein species in the cell appear to increase exponentially during the cell cycle, being synthesized in proportion to cell volume. In principle, a cell could use one of these protein species as a proxy for all of them to determine that its content is approximately doubled before committing to division. We refer to this idea as the threshold accumulation model. A caveat here is that a cell cycle checkpoint is not at the division but at the onset of constriction[11,36], and no cell size adder between consecutive constriction initiation events has been reported.

In addition to approximately doubling its protein content, the cell needs to have a mechanism to verify that it has at least two copies of chromosomal DNA. Accordingly, one would expect the onset of division to be tightly coupled to the replication cycle[31,34,37–39]. However, the tight coordination between replication and division cycles has been disputed[10,35,40]. Recent experiments and analysis have reconciled these views, indicating that the replication status appears to be only one of the input signals for the onset of constriction, and its effect becomes smaller at faster growth rates[11,36]. These ideas are captured in the concurrent processes model, where a replication-related signal and threshold accumulation of an effector protein must both be present to trigger cell division[41,42]. The model leaves open what could be the actual effector protein. Si et al. proposed it to be FtsZ because the adder correlations weakened in cells with downregulated FtsZ amount[35]. These authors furthermore found that the simpler threshold accumulation model was sufficient to describe their data. However, their work did not quantify the downregulated FtsZ amount, and it was carried out in cells where the native FtsZ was replaced by FtsZ fluorescent fusion. It is expected that a sufficient downregulation of any of the essential divisome proteins and likely also non-essential ones would lead to a delay in the onset of constriction, to longer cells and a decrease in the adder correlations. A more conclusive determination of whether the amount of FtsZ or some other division protein is limiting for the cell division is therefore warranted.

Here, we investigate what is the rate-limiting component or process for the onset of constriction in *E. coli* at moderately fast growth rates using high throughput imaging in microfluidic devices and cell cycle modeling. We consider the protein concentration rate-limiting if its increase within the physiologically occurring range significantly accelerates the onset of constriction, at least transiently. Our data and modeling show that FtsZ is rate-limiting for the onset of constriction, while FtsN is not. However, at high excess levels, FtsN does accelerate the onset of constriction. Furthermore, our data also show that FtsA is not rate-limiting nor inhibitory in physiological conditions, but it becomes inhibitory at 50% overexpression level. We propose a model for the onset of constriction that is consistent with these findings.

Results

Our goal in this work was to develop a quantitative approach to determining if a protein is rate-limiting for cell division. A decrease in concentration/protein numbers of the rate-limiting component should lead to delays in the cell division. However, a sufficiently large downregulation of an essential divisome component leads to the cessation of the division process even if this component is not rate-limiting in normal growth conditions[43]. The downregulating concentration of an essential but not rate-limiting protein for cell division, by say 20%, may delay the division process, but at 10%, downregulation may still not be limiting. Controlled and quantitative downregulation of this level of accuracy has not been achieved yet. Therefore, instead of downregulating, we rationalized that upregulation of the protein of interest should produce a more robust way of assessing if it is rate-limiting for cell division. An upregulation within the physiologically occurring range should lead to a temporary increase in the initiation rate of cell divisions if the component is rate-limiting and have no effect if the component is not rate-limiting. The caveat here is that a high upregulation is known to lead to cytotoxic effects. For example, significant overexpression of FtsA and FtsZ alone (more than 7-fold) leads to cessation of cell division[44,45]. Upregulation by a small amount and quantification of this amount is thus necessary. Furthermore, attaching a fluorescent fusion for the protein of interest to quantify its concentration/abundance may affect its function so that the altered protein may become rate-limiting due to its impaired function, as shown below for FtsZ. Having these considerations in mind, we upregulate in our experiments unlabeled protein in wild-type cells (the strain of interest – SOI) and use a strain with a fluorescent proxy on the same chip that expresses a fluorescent protein from the same locus under the same promoter and Shine-Dalgarno sequence (Reporter strain) (Fig. 1a). To calibrate the signal from the fluorescent reporter, we also added a third strain (Reference) which expressed the protein of interest fused to the same fluorescent protein as present in the Reporter strain. The Reference strain expresses this fusion protein constitutively from the native locus of the protein of interest. Using real-time signals from Reporter and Reference allows the calibration of upregulated protein amounts in terms of the native protein concentration (for details, see Methods, Determining Induced Protein Concentrations). We used Western blotting (Supplementary Fig. 1) to validate the method, finding comparable values from the fluorescence-based method and Western blotting (Supplementary Table 5). We mixed SOI, Reporter, and Reference strains for quantitative fluorescence-based measurements and grew cells on a microfluidic mother-machine platform (Fig. 1b, c). After growing the cells for about six generations, we upregulated the protein of interest and monitored the change in protein concentration in the cells (Fig. 1d), cell length at division, Ld, (Fig. 1e), and the doubling time, Td, (Fig. 1f) as a function of time from the upregulation of the protein of interest. We also determined timing, Tc, and the cell length, Lc, at the onset of constriction (Supplementary Fig. 2).

The data in Fig. 1e–f and Supplementary Fig. 2 is pertinent to the upregulation of FtsZ from an extra copy from the λ-attachment (*attB*) site in moderately fast growth conditions in a glucose-CAS medium. FtsZ upregulation by 1.96x (excess FtsZ 96%) leads to a step-like decrease in cell length by about 8% (Fig. 1e) and a transient decrease in doubling time (time from cell birth to next division), with the shortest doubling times being 13% shorter than before the protein upregulation (Fig. 1f). The observed speed-up in cell division frequency is qualitatively consistent with the idea that FtsZ is rate-limiting for cell division in *E. coli* at faster growth rates. At the same time, we did not observe significant changes in cell lengths and cell cycle timings as a result of

https://doi.org/10.1038/s41467-024-54242-w

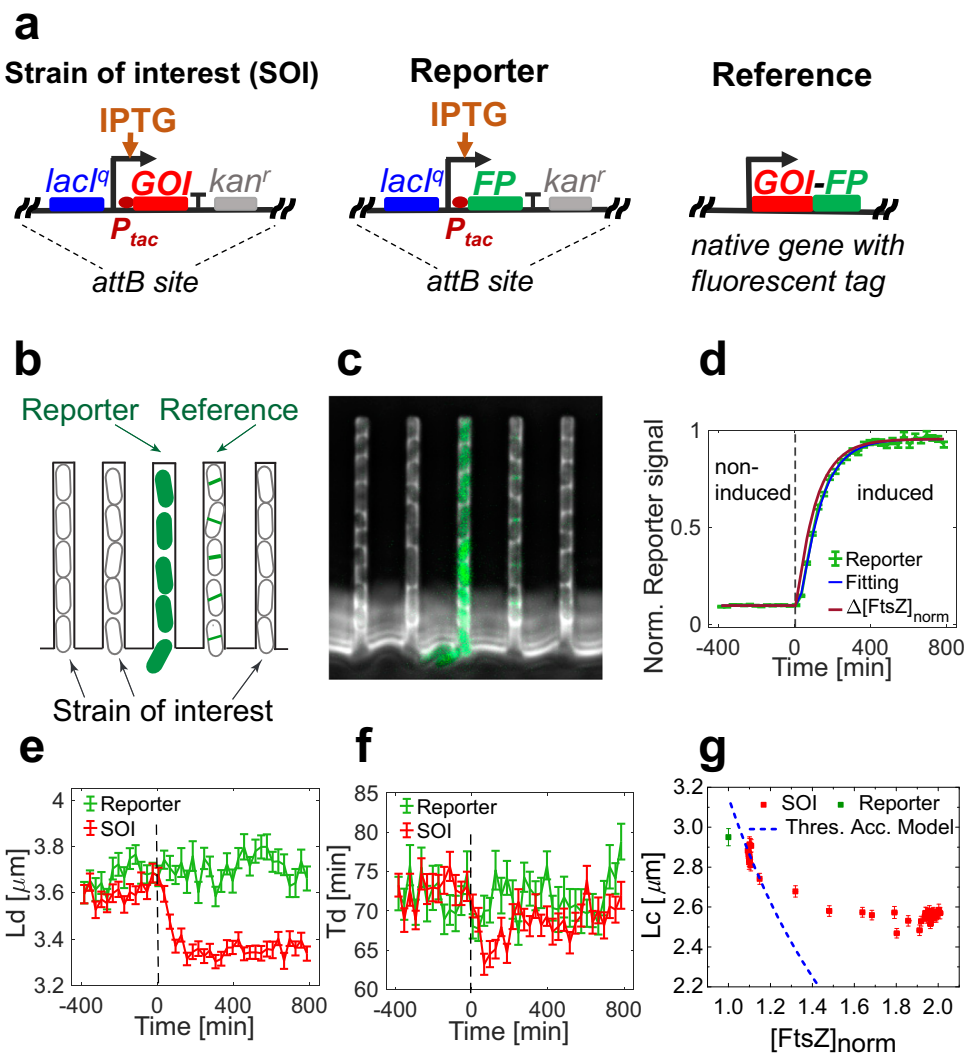

Fig. 1 | Determining proteins that are rate-limiting for cell division. **a** Experimental design. The Strain of interest (SOI), Reporter, and Reference strains were measured simultaneously to determine the effect of upregulation on cell cycle parameters and to quantify the amount of protein produced. SOI expresses an unlabeled gene of interest (GOI) and the Reporter expresses a fluorescent protein (FP) from the same promotor. The Reference strain expresses a native protein of interest with the same fluorescent fusion as the Reporter. For a list of all SOI, Reference, and Reporter strains used in experiments see Supplementary Table 4. **b** Schematics of the microfluidic device. The three strains in experiments were mixed and grown on the same microfluidic mother-machine device. **c** A snapshot image of the device after upregulation of the protein of interest, which in this image is FtsZ. **d** Increase of fluorescent reporter signal (Reporter) due to its induction. Addition of IPTG inducer (500 μM) at time zero is indicated by a dashed vertical line. The curve of the Reporter is normalized by the Reference signal (green points). The blue line is fitting of the fluorescence induction model to the data and the dark red line is the calculated excess normalized concentration of FtsZ, which is corrected for fluorophore maturation (for details, see Methods, Fluorescence induction model to determine protein concentrations). The fitting shows 96% excess FtsZ concentration compared to this concentration in WT cells, corresponding to the final $[FtsZ]_{norm} = 1.96$x. **e** The cell length at division as a function of measurement time for SOI (red) and Reporter (green). **f** The doubling times for the same cells. **g** Cell length at the onset of constriction versus the normalized concentration of FtsZ. The red points show data from SOI, and the green point corresponds to the Reporter strain. The dashed line represents the threshold accumulation model. The number of analyzed cells in panels **d**–**g** is $N = 7817$ for the SOI and $N = 4948$ for the Reporter strain. All error bars correspond to s.e.m. Source data are provided as a Source Data file.

FtsZ upregulation in slow growth rates in an alanine medium even at a much higher upregulation level (Supplementary Fig. 3). This finding is consistent with our earlier works[11,36] which show that replication-related processes are dominantly rate-limiting for *E. coli* cell division at slow growth rates rather than processes arising from protein abundances.

Since the focus of this work is to understand rate limitations arising from protein abundances, the remainder of the work deals with moderately fast growth rates. Comparing the data in Fig. 1d and e, obtained at a moderately fast growth rate, shows that at higher overexpression levels, FtsZ ceases to be rate-limiting because changes in cell length stop about 100 min after the start of the induction, while the FtsZ concentration continues to increase further for about 200 min. The cessation of FtsZ being rate-limiting during the upregulation can be more clearly seen by plotting cell length as a function of the normalized FtsZ concentration, $[FtsZ]_{norm}$, (Fig. 1g). Note that $[FtsZ]_{norm}$ is based on the normalized reporter signal, which is corrected for fluorophore maturation effects (see Methods). Here, we chose to measure the cell length at the onset of constriction rather than at the division because the former is the cell cycle checkpoint. The data show that as $[FtsZ]_{norm}$ starts to increase, the cell length at constriction decreases linearly in time, but when $[FtsZ]_{norm}$ exceeds about 1.7x of the native level, the decrease stops. This is approximately the point when FtsZ ceases to be rate-limiting for triggering the onset of

constriction for all the cells in the cell population. To explain the changes in cell length upon FtsZ upregulation quantitatively, we compared the data to the FtsZ threshold accumulation model proposed earlier[35] but with a modification that the FtsZ number threshold is reached at the onset of constriction rather than at the division (Fig. 1g). Assuming the FtsZ concentration in this growth condition is constant during the cell cycle yields a simple prediction $Lc = Lc^{WT}/[\mathrm{FtsZ}]_{\mathrm{norm}}$ as indicated by a dashed line in Fig. 1g. Here Lc^{WT} is the cell length in WT cells without extra FtsZ. The prediction differs in two aspects from the experimental data: 1) the predicted line does not show a plateau at higher $[\mathrm{FtsZ}]_{\mathrm{norm}}$ values and 2) the slope of the curve at a small $[\mathrm{FtsZ}]_{\mathrm{norm}}$ is much higher than in the data.

We also performed upregulation measurements with two strains where the native FtsZ was replaced by FtsZ sandwich fusion to fluorescent mNeonGreen, FtsZmNG[46]. In one of these strains, the extra inducible copy inserted in the *attB* site carried FtsZmNG, while in the other strain, it contained the unlabeled FtsZ (as in SOI). Both strains were about 25% longer than the unlabeled SOI, consistent with earlier report[46]. Upon upregulation of FtsZ, the cell length of both FtsZmNG labeled strains decreased about three times more than unlabeled SOI, reaching as a result of upregulation about the same length as the WT cells (Supplementary Fig. 4a–d). Comparing cell lengths vs $[\mathrm{FtsZ}]_{\mathrm{norm}}$ data from these curves to the threshold accumulation model showed that this model better fit the data from the labeled than from the unlabeled strain (Supplementary Fig. 4e–f). These results suggest that a fluorescent fusion to FtsZ reduces its functionality, and the reduced functionality of FtsZmNG makes it more limiting than the WT FtsZ for the onset of constriction. However, the cell length defect can be corrected by higher expression of FtsZmNG. The above comparison also potentially explains why an earlier work[35], where a strain with FtsZ sandwich fusion was used, concluded that the FtsZ threshold accumulation model applies.

The concurrent process model approximately explains the data

The plateau region in cell length vs $[\mathrm{FtsZ}]_{\mathrm{norm}}$ data in unlabeled SOI strain indicates that in addition to FtsZ accumulation, there could be an additional process that controls the onset of the constriction. This idea is captured by the concurrent processes model[36,41,42], where one of the limiting processes stems from FtsZ numbers reaching a threshold value in the cell, and the other limiting process originates from the DNA replication cycle. To compare the model to the experimental data, we used cell cycle parameters determined from the experiments and adjusted the threshold level for the FtsZ numbers and the time duration when the replication-related processes block the onset constriction using the measurement shown in Fig. 1d–g (for details see Methods, Modeling). After these adjustments, the model quantitatively explained the increase in fluorescent protein concentration from the Reporter (Fig. 2a), step-like decrease in cell length (Fig. 2b, Supplementary Fig. 5a), and the transient decrease in timings for the onset of constriction (Fig. 2c) and cell division (Supplementary Fig. 5b). Note that to reproduce the change in steady state timings for the onset of constriction (Tc) we needed to account for the increased constriction period ($\Delta Ts = Td - Tc$) that resulted from FtsZ upregulation (Supplementary Fig. 6).

Qualitatively, the cell length and transient decrease in timings for the onset of constriction and division can be understood in the model because, at the higher synthesis rate of FtsZ, the cells reach the number threshold earlier in the cell cycle when their length is smaller. However, as the cells get smaller, the synthesis rate of FtsZ, which is proportional to cell volume/length, decreases. The timings Tc and Td, therefore, shift back to their original values after the completion of one whole cell cycle that follows the upregulation of FtsZ (without accounting for increased ΔTs). The unchanged steady state timings Tc and Td after upregulation of FtsZ from their pre-induction values can also be understood from the constancy of cell growth rates before and after upregulation. However, as mentioned above, we adjusted the basic model for the increased constriction period ($Td - Tc$), which accompanies FtsZ upregulation. The increased constriction period shortens both Tc and Td because more FtsZ accumulates during the longer constriction period in the previous cell cycle.

To test the model further, we carried out additional experiments where FtsZ concentration at the final steady state differed from the one shown in Fig. 2a–c. The model predicts that because of the increase in the final FtsZ steady-state concentration, the change in cell length at constriction approaches a minimal limiting value, and the duration of cell length change decreases (Fig. 2d). The minimal limiting length is determined by replication-related processes alone. Without any further parameter adjustments, the model qualitatively predicted the time-dependences of all measured quantities in both overexpression conditions (Fig. 2e–f, Supplementary Fig. 7, 8). At the quantitative level, however, the experimentally observed effect was smaller than the model prediction for the cell lengths at the onset of constriction in the low overexpression conditions (1.57x) (Fig. 2e). The same was true also for the higher (3.2x) overexpression measurement (Fig. 2f). However, in this measurement, the effect appeared as incorrectly predicted Lc value before upregulation. This is because, before the upregulation of FtsZ, there was a smaller leaky expression of FtsZ in high (3.2x) overexpression measurement ($[\mathrm{FtsZ}]_{\mathrm{norm}} = 1.02$x) compared to the two lower FtsZ overexpression measurements ($[\mathrm{FtsZ}]_{\mathrm{norm}} = 1.10$x). The model was thus unable to quantitatively predict the effects arising from this leaky expression. The failure of the model to correctly predict cell length due to leaky expression of FtsZ was also evident when we compared the cell lengths from the Reporter strain, which has a native level of FtsZ, to the model (Supplementary Fig. 9). The behaviors in all overexpression levels can be summarized in the FtsZ titration plot (Fig. 2g). The model can be seen to fit the data well, except for the $[\mathrm{FtsZ}]_{\mathrm{norm}} \lesssim 1.1$x and for $[\mathrm{FtsZ}]_{\mathrm{norm}} \gtrsim 2.3$x. The deviation of the model for $[\mathrm{FtsZ}]_{\mathrm{norm}} \gtrsim 2.3$x could be explained by the onset of cytotoxic/inhibitory effects of FtsZ overexpression, as has been observed earlier at higher expression levels[44]. Furthermore, at $[\mathrm{FtsZ}]_{\mathrm{norm}} = 3.2$x overexpression levels, about 1% of all divisions lead to mini cells, which is not accounted by the model. We did not observe mini cells at two lower overexpression levels.

While the deviation of the model from the experiments for $[\mathrm{FtsZ}]_{\mathrm{norm}} \gtrsim 2.3$x was expected, the discrepancy at $[\mathrm{FtsZ}]_{\mathrm{norm}} \lesssim 1.1$x presents a more significant challenge for the model. A key characteristic of the concurrent processes model is a large cell length change for variations in FtsZ concentration close to $[\mathrm{FtsZ}]_{\mathrm{norm}} = 1.0$x and decrease of this response as $[\mathrm{FtsZ}]_{\mathrm{norm}}$ increases (Fig. 2g). Such behavior is independent of model parameters. Failure of this prediction suggests that a number threshold postulated by the model may not accurately capture cellular response near the WT concentration of FtsZ. Instead of a simple number-sensing mechanism, there could be a more complex response function involved in the decision-making process that triggers the onset of constriction. At the same time, the model fits the data well at high overexpression conditions, suggesting that at a coarser level, the accumulation to threshold number provides a good, effective model to explain how the onset of constriction is triggered.

Quantifying FtsZ limitation

A comparison of data and model shows that the FtsZ amount in the cell is one of the rate-limiting factors for the onset of constriction. The question then arises: how limiting is FtsZ? As mentioned above, the concentration-dependent decrease in cell length plateaued at about 1.7x overexpression levels of FtsZ (Fig. 2g), indicating that at this overexpression level, FtsZ is effectively not limiting the onset of constriction for any cell in a population. Alternatively, the concurrent processes model allows us to estimate the probability that in each division FtsZ numbers are limiting the onset of constriction. This probability as a function of $[\mathrm{FtsZ}]_{\mathrm{norm}}$ is shown in Fig. 2h. The

https://doi.org/10.1038/s41467-024-54242-w

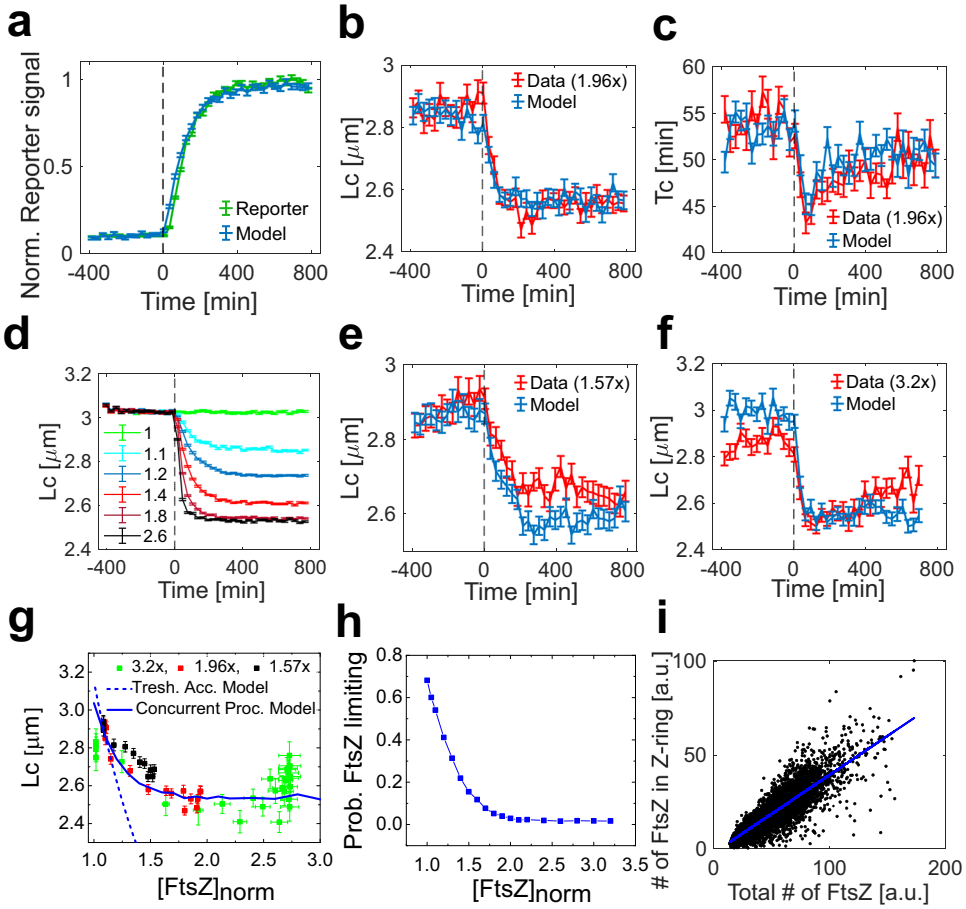

Fig. 2 | Comparing the experiment and the concurrent processes model. a–c The normalized reporter signal (green), the cell length, and the timing of the onset of constriction from the experiment (red) and model (blue). The experimental curves correspond to the measurement in Fig. 1. **d** Model predictions for cell length at the onset of constriction for different levels of upregulation of FtsZ. The legend shows the final steady-state value of $[FtsZ]_{norm}$ for each curve. **e**, **f** Comparing model predictions for *Lc* to measurements where the final steady-state value is $[FtsZ]_{norm} = 1.57x$ and $[FtsZ]_{norm} = 3.20x$, respectively. For comparisons of other measured quantities, see Supplementary Figs. 7 and 8. The number of cells analyzed is $N = 8609$ for 1.57x (Panel **e**) and $N = 6909$ for 3.2x upregulation measurements (Panel **f**). **g** *Lc* vs $[FtsZ]_{norm}$ from three FtsZ upregulation measurements combined. The blue solid line is the prediction from the concurrent process model, and the dashed line is from the threshold accumulation model. **h** The probability that FtsZ numbers limit the onset constriction in a cell population according to the concurrent processes model. **i** The total number FtsZ in the Z-ring vs the total number of FtsZ in the cell from measurements in FtsZmNG labeled strain JM276. The data before and throughout the upregulation of FtsZmNG to the final value 1.62x are both plotted from cell cycle times from Tz, per to $0.9Td$. The solid line is a linear fit with a slope of 0.42 and an intercept of -2.1. Pearson $R = 0.89$. The number of datapoints is 24769. All error bars correspond to s.e.m. Source data are provided as a Source Data file.

probability approaches zero at $[FtsZ]_{norm} \approx 1.7x$ as expected from the previous argument. More importantly, the model predicts that FtsZ is limiting in 68% divisions for the WT cells at the native level of FtsZ (i.e. $[FtsZ]_{norm} = 1.0x$). It is worth emphasizing that this number is as valid as the model. Since the model shows a smaller change in cell lengths than the experiment at low overexpression levels of FtsZ, 68% probability is likely an overestimate. Nevertheless, we can draw a rough estimate that for at least half of the cell divisions in WT cells in this moderately fast growth condition, FtsZ numbers in the cell rate limit the onset of constriction.

Proportionality of FtsZ numbers in the cell to FtsZ numbers in the Z-ring

Our analysis and modeling so far have focused on the total number of FtsZ molecules and their concentrations in the cell. While this quantity is sufficient to determine if FtsZ is rate-limiting for the onset of constriction, the relevant molecular processes occur in the Z-ring. Therefore, FtsZ numbers in the Z-ring are also of interest. To investigate the relationship between FtsZ numbers in the Z-ring and total FtsZ numbers in the cell, we studied cells where the native *ftsZ* locus was replaced with the FtsZmNG fusion variant. These cells also had inducible extra copy FtsZmNG (strain JM276) or native FtsZ (strain JM275) expressed from the λ-attachment site as described earlier (Supplementary Fig. 4). As previously noted, these cells were longer than WT cells (Supplementary Fig. 4c). However, upregulating FtsZmNG by 1.62x shortened the cells to approximately WT sizes, mitigating the apparent defect. In the majority of cells, the new Z-ring started to assemble concurrently with the dissociation of the Z-ring in the mother cell, as reported before[7]. However, the initial assembly can be transient in individual cells, with the Z-ring intermittently dissociating[47]. We, therefore, defined two time points related to the assembly of the Z-ring: $Tz,1$ marks the earliest time from cell birth when the first FtsZ assembly is present at the midcell, and Tz, per the earliest time when a persistent Z-ring is present, remaining until the cells are about to divide. The distributions of $Tz,1$ and Tz, per were both peaked at $Tz = 0$ with a tail to longer times (Supplementary Fig. 10a,b). Since the Z-ring formation mostly coincides with the dissociation of the old Z-ring in the mother cell, upregulation of FtsZmNG by 1.62x had a limited effect on either of these Tz values (Supplementary Fig. 10a–c, f). The upregulation of FtsZ in these cells thus transiently shortened

the delay from the Z-ring formation to the onset of constriction (Supplementary Fig. 10d, e, g, h). This finding indicates that FtsZ concentration in the cell directly affects the onset of constriction rather than accelerating Z-ring formation and thereby indirectly speeding up all downstream processes.

We then determined the total number of FtsZ in both the cell and in the Z-ring, where the latter was present (see Methods, Determining the Z-ring and N-ring-related parameters). The two numbers showed a high correlation ($R = 0.89$) for all cells with a detectable Z-ring, for a cell cycle period spanning from Tz, per to $0.9Td$ (Fig. 2i, Supplementary Fig. 11a, b). Note that for most cells $0.9Td > Tc$. The correlation between the total numbers of FtsZ molecules in the cell and those in the Z-ring was lower during the early and late stages of the cell cycle (Supplementary Fig. 11c, d). The same conclusion can be drawn from a different analysis where the excess FtsZ numbers at the midcell were correlated with the total number of FtsZ in the cell irrespective if the cells had a Z-ring or not (Supplementary Fig. 11e–h). These findings show that the amount of FtsZ in the Z-ring is determined by the total number of FtsZ in the cell throughout most of the cell cycle, except for a fraction of cells in early cell cycle stages without Z-ring and in the latest stages ($T > 0.9Td$) when the Z-ring started to dissociate. Therefore, the accumulation of FtsZ numbers to a threshold value in the cell, as postulated in the threshold accumulation and concurrent processes models, can be considered equivalent to the accumulation of FtsZ numbers to a threshold value in the Z-ring.

FtsN is not rate-limiting for the onset of constriction

Our modeling considered replication the second limiting process, but similar results can be obtained if, instead of replication, another division-related protein limits the onset of constriction (Supplementary Fig. 12). Our earlier data indicate that at moderately fast growth conditions, as used here, replication is only a modestly limiting factor for the onset of constriction[11,36]. Several recent works have argued that FtsN acts as a trigger for the onset of constriction[13–15,17–20,48]. Therefore, we also carried out the upregulation measurements for FtsN. In the first set of measurements, we upregulated FtsN concentration by about 71% (Fig. 3a), which is similar to the FtsZ overexpression level in Fig. 1. Unlike for FtsZ, there was no systematic change in Ld, Lc, Td or Tc upon overexpression of FtsN (Fig. 3b, c, Supplementary Fig. 13a, b). In a two-sided Mann-Whitney test, Lc and Ld before and after upregulation were not statistically significant (p-value > 0.2). We then repeated the measurements at a much higher upregulation level of FtsN (7.56x, Fig. 3d). In this case a clear decrease in cell length appeared (Fig. 3e, Supplementary Fig. 13c, d) as observed earlier[49].

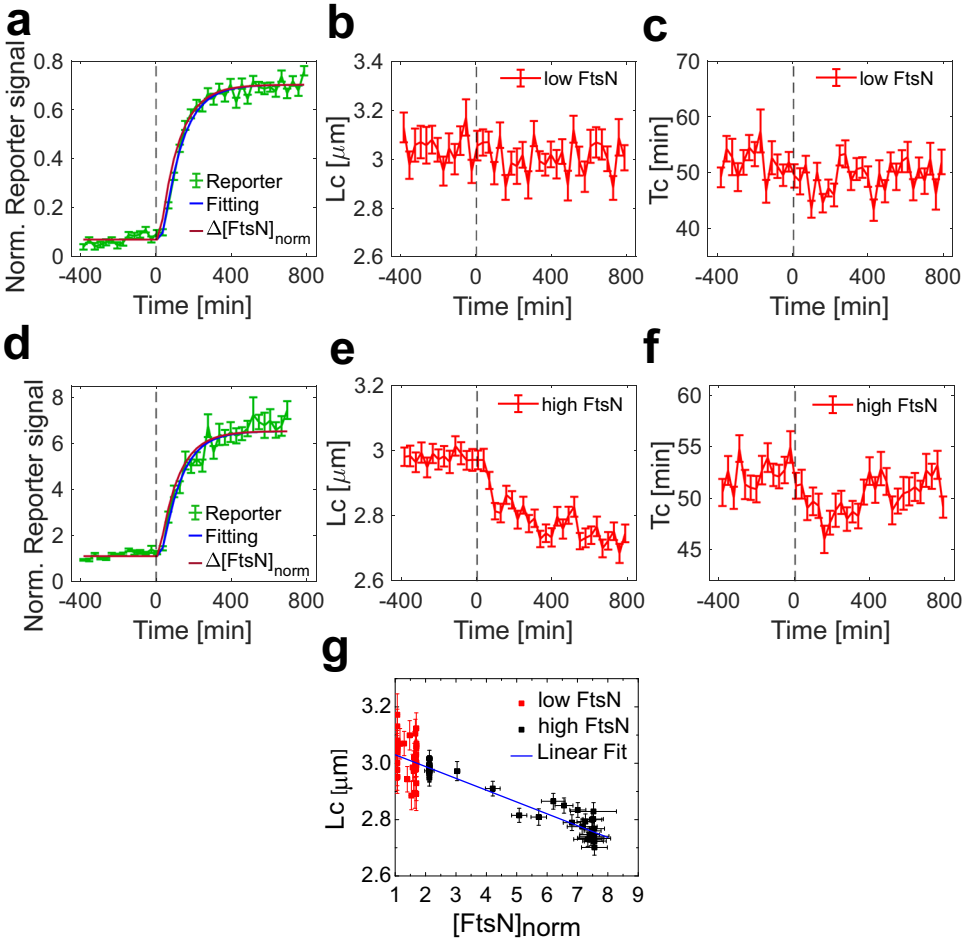

Fig. 3 | Upregulation measurements of FtsN. a Increase of fluorescent reporter signal (Reporter) due to low level (71%) overexpression corresponding to the final $[FtsN]_{norm} = 1.71x$ (comparable to FtsZ upregulation measurement in Fig. 1). The curve is normalized by the Reference signal. The blue line fits the fluorescence induction model to the data, and the dark red line is the calculated total upregulated protein concentration. The number of analyzed cells is $N = 7556$. **b, c** The cell length at the onset of constriction and the timing for the onset of constriction as a function of time ($N = 2478$), respectively in this measurement. Time zero corresponds to adding IPTG inducer (indicated by a dashed vertical line). **d–f** The same measurements as in the top row but for a high level of upregulation corresponding to the final $[FtsN]_{norm} = 7.56x$. $N = 3856$ for the Reporter and $N = 8871$ for SOI. **g** Lc vs $[FtsN]_{norm}$ from these two FtsN upregulation measurements combined. The solid line is a linear fit to the data with slope of $-0.042\mu m^{-1}$ and intercept of 3.0μm. All error bars correspond to s.e.m. Source data are provided as a Source Data file.

Combining these measurements in the FtsN titration curve showed that cell length decreased approximately linearly with $[FtsN]_{norm}$ throughout the entire studied range (Fig. 3g). However, the response of cell lengths to changes in $[FtsN]_{norm}$ was about ten times less sensitive than to changes in $[FtsZ]_{norm}$. The same decrease in cell length was observed with the 7.56x upregulation of FtsN as with the 1.71x upregulation of FtsZ. To put these numbers into perspective, we determined FtsN concentration in the cell cycle using previously reported Ypet-FtsN construct[9]. We estimate that the average concentration varies only about ±2% (±0.02x) around its population-average value during the cell cycle (Supplementary Fig. 14a). At the same time, FtsN concentration at the onset of constriction varies by 23% (0.23x) in the cell population (Supplementary Fig. 14b). Considering the latter number as the natural variation of $[FtsN]_{norm}$ and using the slope from the titration curve in Fig. 3g shows that the FtsN variation in the cell population can account only for 10 nm variation in *Lc* while the variation (standard deviation) of *Lc* in cell population is 470 nm. Altogether, FtsN accelerates cell division at very high overexpression levels, but it is not rate-limiting the onset of constriction under normal growth conditions.

We also carried out FtsN upregulation measurements in a fluorescent fusion strain where a native copy of *ftsN* was replaced with *Ypet-ftsN* and an extra inducible *Ypet-ftsN* was cloned to the λ-attachment site. While the upregulation of Ypet-FtsN does not also accelerate the onset of constriction at moderate expression levels (the final $[FtsN]_{norm} = 1.48x$, Supplementary Fig. 15a–e), the excess Ypet-FtsN at midcell nevertheless increases in these conditions (Supplementary Fig. 16a). The fold-increase in the midcell Ypet-FtsN is larger in the late stages of the cell cycle (Supplementary Fig. 16b), similar to the increase in FtsZmNG when the latter is upregulated (Supplementary Fig. 16c, d). However, because of upregulation, excess Ypet-FtsN is also present at the midcell (N-ring) during the early cell cycle (Supplementary Fig. 16b). As observed previously in FtsA* (R286W) mutant cells[9], the measurement here in WT FtsA background shows that earlier FtsN accumulation at midcell (Supplementary Fig. 15f, g) does not trigger the earlier onset of constriction (Supplementary Fig. 15d, e). The latter finding further supports the conclusion that FtsN is not rate-limiting for the onset of constriction.

A low level of FtsA overexpression is not inhibitory

FtsA is the second most conserved bacterial cell division protein besides FtsZ[50]. At several-fold upregulation, FtsA is cytotoxic, preventing the onset of constriction[45,51]. However, it is possible that at native levels, it is rate-limiting for cell division like FtsZ because the two proteins are expressed from the adjacent genes in the same operon. To test this hypothesis, we carried out overexpression measurements also for FtsA (Fig. 4a). Contrarily to our hypothesis, FtsA in low overexpression conditions (the final $[FtsA]_{norm} = 1.6x$) did not lead to a change in cell length and timing of the onset of constriction (Fig. 4b, c) and of these parameters at the division (Supplementary Fig. 17a-b), suggesting that FtsA is not rate-limiting for cell division in normal growth conditions. However, higher overexpression levels of FtsA (the final $[FtsA]_{norm} = 2.4x$) led to an increase in cell length (Fig. 4d, Supplementary Fig. 17d) but not the timing of the onset of constriction (Fig. 4e, Supplementary Fig. 17c). The length increase only occurred after a distinct delay (Supplementary Fig. 17e), confirming that at the low level of overexpression, FtsA is not inhibitory. The increase in cell length at higher overexpression levels is consistent with earlier reports[9,45,51]. Converting the time-dependent measurements to the FtsA titration curve showed that FtsA inhibitory effects set in at about 1.6-1.7x overexpression levels (Fig. 4f). A 1.6-1.7x overexpression of [FtsA] beyond its mean value is likely beyond the natural variation in a cell population as it is for FtsN. So, in a population, FtsA is not expected to be inhibitory for the vast majority or even in any cells in the population in regular growth conditions.

The above data showed that while the cell length increased at high FtsA overexpression levels, there was effectively no change in the timing for the onset of constriction. To understand why the increase in cell length is not accompanied by a transient increase in the timing for the onset of constriction, we modeled the FtsA upregulation measurements using the concurrent processes model. We considered an increase in [FtsA] to lead to a higher threshold level for FtsZ numbers at which they trigger the constriction. We assumed that the increase in the threshold level is proportional to the excess [FtsA], but only above $[FtsA]_{norm} = 1.6x$ (based on Fig. 4f). Apart from this change, the model and the parameters were the same as in Fig. 2. The model reproduced the experimentally observed increase in cell lengths (Fig. 4d, Supplementary Fig. 17c). Notably, the model also showed, consistent with the experiment, that the timing for the onset of constriction was effectively unchanged (Fig. 4e, Supplementary Fig. 17d). There is no distinct increase in *Tc* in the model because the threshold level for FtsZ to trigger the onset of constriction gradually increases as more FtsA is produced. The gradual increase in threshold level smears out the transient change in *Tc* in a population average measurement. In contrast, in FtsZ upregulation measurements, the synthesis rate of FtsZ abruptly increases upon induction, and a transient change in *Tc* can be observed. Interestingly, while the upregulation of FtsZ leads to a longer constriction period (Supplementary Fig. 6), the high level of upregulation of FtsA (the final $[FtsA]_{norm} = 2.4x$) shortens it (Supplementary Fig. 17f) even though at this level of overexpression, FtsA has an inhibitory effect on the onset of constriction.

Unlike FtsA, overexpression of its hypermorphic mutant FtsA* (R286W) is not known to cause cytotoxic effects and leads to short cell phenotype[52]. To quantify its effects, we also upregulated FtsA* in the WT FtsA background (about 2.4x; Fig. 4g). Upregulation led to decreased cell length (Fig. 4h, Supplementary Fig. 18a–d) and a transient decrease in the timing for the onset of constriction that did not recover fully (Fig. 4i). The effect appeared in all aspects very similar to the ones from FtsZ upregulation measurements. We overlayed the two measurements (Supplementary Fig. 18e-h), finding the effects of FtsZ and FtsA* upregulation almost indistinguishable from each other. Note the *Ld* vs Time and *Td* vs. Time curves are insensitive to the amounts of protein upregulation in the range of concentrations (cf. Fig. 2d). Since FtsZ and FtsA* have the same downstream effect, they may cause the same change in the divisome that is needed to trigger the onset of constriction.

Discussion

Key proteins in the cell division in *E. coli* are the earliest-arriving components FtsZ and FtsA, and the last arriving essential protein FtsN. Here, we investigated if any of them are rate-limiting for cell division by modestly upregulating their concentrations. Although the upregulation of these proteins has been carried out in the past, the increase of protein concentrations in these measurements frequently far exceeded the physiologically relevant range and had not been precisely quantified. Furthermore, cell length and division timings have been inferred at the time of division rather than at the onset of constriction. Such measurements overlook the possibility that increased levels of some proteins can change the constriction period in addition to timing for the onset of constriction, as we observe for FtsZ (Supplementary Fig. 6) and FtsA (Supplementary Fig. 17c-f). By addressing these limitations, our measurements presented here show that FtsZ is rate-limiting for cell division at moderately fast growth conditions, whereas FtsN and FtsA are not.

While the rate-limiting role of FtsZ in faster growth rates is expected based on earlier works[44,53], the finding that FtsN is not rate-limiting refutes the idea that it is the trigger protein. This notion does not mean that FtsN is not needed/essential for the onset of constriction. Based on the terminology proposed earlier[43], FtsN is a secondary rather than a primary cell cycle regulator. Clearly, the depletion of FtsN

https://doi.org/10.1038/s41467-024-54242-w

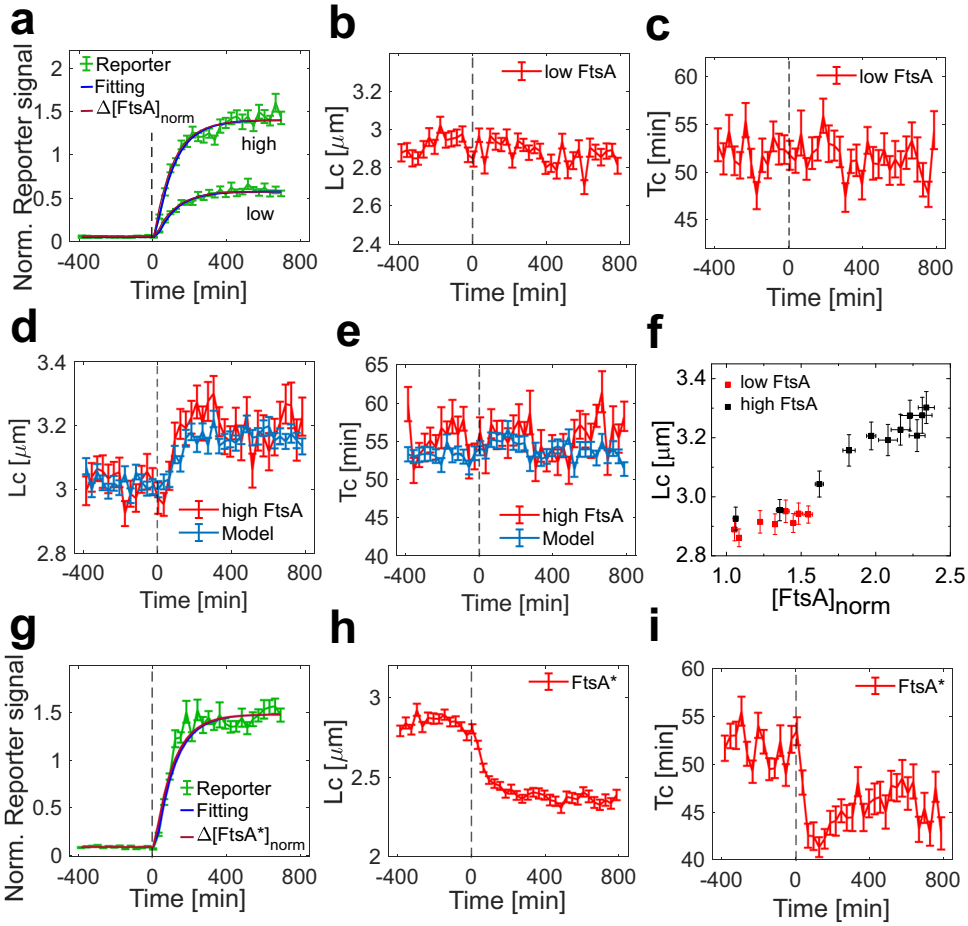

Fig. 4 | Effects of overexpression of FtsA and FtsA*(R286W). a Increase of fluorescent reporter signal (Reporter) as a result of its induction at a low level of upregulation (1.6x = 60% excess) and a high level of upregulation (2.4x = 140% excess). The blue line fits the fluorescence induction model to the data, and the dark red line is the calculated total upregulated protein concentration. The number of the Reporter cells analyzed for the high overexpression measurement is $N = 1788$ and for the low $N = 3035$. **b**–**c** Cell length at the onset of constriction and its timing vs the measurement time for the final $[FtsA]_{norm} = 1.6x$. $N = 5367$. **d**–**e** Cell length at the onset of constriction and its timing vs the measurement time for the final $[FtsA]_{norm} = 2.4x$ (red lines). $N = 5012$. The blue lines are from the concurrent processes model where the threshold numbers for FtsZ increase in proportion $[FtsA]_{norm}$ once the latter reaches 1.6x. **f** The average cell length at the onset of constriction versus $[FtsA]_{norm}$ from the two measurements combined. **g** Increase of fluorescent reporter signal (Reporter) as a result of its induction in FtsA*(R286W) overexpression measurement. The blue line fits the fluorescence induction model to the data, and the dark red line is the calculated total upregulated protein concentration. $N = 2995$. **h, i** Cell length at the onset of constriction and timing vs the measurement time for the final $\left[FtsA^*\right]_{norm} = 2.4x$. $N = 6758$. All error bars are s.e.m. Source data are provided as a Source Data file.

leads to the cessation of cell division. However, it is present in the cell in excess concentration and ready to be incorporated into the divisome complex early on in an FtsA* background as was demonstrated earlier[9]. The results from this earlier work, thus, showed that FtsN is not sequestered away by some yet-to-be-identified protein interactions in earlier stages of the cell cycle or undergoing some post-translational modifications before the onset of constriction. Instead, there is some other change in the upstream complex that needs to occur before FtsN can bind to the complex. Rather than being a trigger to the onset of constriction, the binding of FtsN to the divisome complex appears to be a consequence of some other event occurring before FtsN binds to FtsA.

What could this event be? Our data indicates that increase in FtsZ numbers in the cell and in the Z-ring drives this transition. We used a previously published FtsZ polymerization model[54] to understand what effect an increase in FtsZ numbers and concentration has on FtsZ protofilaments. Based on modeling, the excess [FtsZ] leads to an increased number of FtsZ protofilaments (Supplementary Fig. 19). The increase in filament number is approximately proportional to the increase in FtsZ concentration. At the same time, the increase in concentration changes the filament length only weakly. More filaments of approximately the same length can be expected to lead to elevated filament bundling. Based on these arguments, we can infer that FtsZ protofilament bundling is needed for the onset of constriction.

There are several possibilities of what effect FtsZ protofilament bundling may have. A high local concentration of FtsZ protofilaments due to bundling may cause a small inward bending of the plasma membrane, which may be needed to initiate septal peptidoglycan synthesis. The bending would be mediated by FtsA and ZipA. FtsA might have a dominant effect over ZipA because of its shorter disordered linker, which would bear a majority of the load from bending intrinsically curved FtsZ protofilaments[55]. It remains, however, unclear how the excess of FtsA could hinder and the excess of FtsA* mediate the force transduction. Furthermore, the magnitude of the bending may not be significant in vivo, where the turgor pressure could oppose membrane deformations.

Alternatively, FtsZ protofilament bundling can enforce a conformational change in FtsA, which in turn activates septal peptidoglycan synthesis. Recent data indicate that for the latter to occur, FtsA antiparallel filaments are needed[20]. The same work found that the

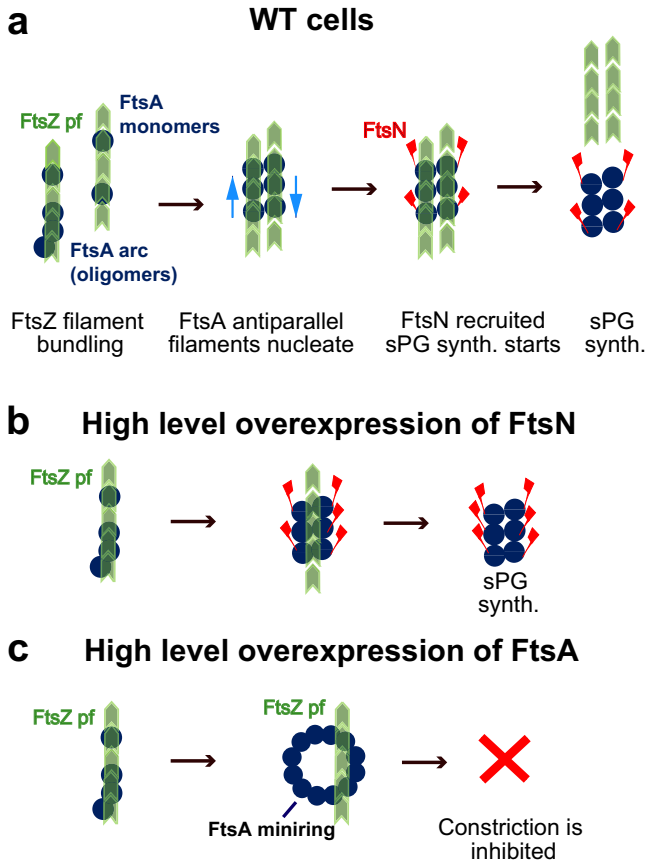

Fig. 5 | A proposed mechanism for the onset of constriction. a In WT cells, an FtsZ protofilament doublet or a larger bundle is needed to nucleate the FtsA antiparallel filament. The nucleated filament is stabilized by FtsN. **b** Unnaturally high concentrations of FtsN can lead to FtsA antiparallel filament formation without FtsZ protofilament doublet. **c** Unnaturally high concentrations of FtsA can lead to FtsA minirings, which prevent FtsZ protofilament bundling and inhibit constriction formation.

transition to antiparallel filaments can be induced by adding high concentrations of FtsN N-terminal cytoplasmic tail to the reaction mixture. Our data indicate that FtsN is not rate-limiting in vivo, while FtsZ is. Accordingly, we propose that the transition to FtsA antiparallel conformation is driven by FtsZ but not by FtsN.

In vivo measurements indicate that FtsA antiparallel filaments are not thermodynamically favored compared to arcs and minirings when only FtsA alone is present in the reaction mixture[20,30]. We postulate that for the formation of a FtsA antiparallel filament, FtsZ protofilaments need to form at least a local doublet to nucleate FtsA antiparallel filaments (Fig. 5a). A straight doublet of FtsZ protofilaments may force monomers and curved FtsA arcs to a straight (antiparallel) filament conformation. In this conformation, 1:1 stoichiometry between FtsZ and FtsA locally holds where every C-terminal tail of FtsZ is bound to FtsA. Based on the proposed model, these FtsZ C-terminal connections to FtsA drive the FtsA antiparallel filament formation. However, FtsZ protofilament doublets need to be parallel to stay together during treadmilling while FtsA oligomers are antiparallel. This appears not to be a contradiction. We expect the free energy difference of FtsZ binding to the FtsA parallel strand compared to the antiparallel strand to be minimal because FtsZ has a long and flexible C-terminal linker. Once FtsA antiparallel filament nucleates, it is further stabilized by binding FtsN to it. The nucleation and antiparallel filament formation can also be driven by FtsN alone without FtsZ doublets and bundles but at much higher concentrations of FtsN than present in cells in vivo (Fig. 5b). The proposed mechanism works as if the arrival of FtsN to the divisome triggers the onset of constriction even though the actual mechanism is the conformational switch of FtsA induced by FtsZ protofilament bundling. The proposed mechanism does not contradict recent single-molecule tracking data where some fraction of FtsBQL and FstIW complexes were found to move together with treadmilling FtsZ protofilaments[21,23]. These complexes can bind to mostly monomeric FtsA and follow treadmilling FtsZ protofilaments by diffusion and capture[25]. Furthermore, FtsZ doublets together with FtsA doublets have been observed in vitro experiments[56] (Fig. 2c in the reference) and can also be inferred from a different study that used an amphipathic helix deletion mutant of FtsA[57].

Alternatively, one could consider a mechanism where the onset of constriction is triggered by the transition of FtsA minirings to its antiparallel filament conformation (Supplementary Fig. 20)[1]. The only difference between the two mechanisms is the initial polymerization state and conformation of FtsA (monomers and FtsA arcs vs minirings). FtsA minirings can be expected to be inhibitory for the onset of constriction because of the occlusion of the FtsW binding interface in this conformation of FtsA[58]. If FtsA minirings were already present in cells in the native expression level of FtsA, then we would expect a continuous increase in cell length as FtsA concentration increases and more and more FtsA minirings form that are not competent for recruiting downstream components. Instead, our data show an inhibitory effect arising from FtsA upregulation only at larger than 1.6x overexpression levels (Fig. 4f). We interpret the onset of inhibitory effects as a threshold for FtsA miniring formation. Consistent with this idea, in vitro measurements have also shown a well-defined threshold for the FtsA miniring formation as the concentration of FtsA increases[27,30].

FtsA* is defective in forming minirings[30], and it was observed to transform more readily to antiparallel filament conformation in vivo in the presence of FtsN[20]. Expression of FtsA* could accelerate the onset of constriction, as observed in our measurements (Fig. 4h), because it prevents short FtsA arcs from forming, and this facilitates the nucleation of FtsA antiparallel filaments. So, its effect is similar to the one we observe in FtsZ upregulated conditions (Supplementary Fig. 18e–h). Within this picture, both FtsA* and FtsZ overexpression facilitate the formation of FtsA antiparallel filaments. FtsA* achieves this by shortening FtsA oligomers and thereby lowering the activation barrier for nucleation of FtsA antiparallel filaments.

Altogether, our data is consistent with the model where an increase of FtsZ numbers in the cell cycle is one of the driving mechanisms for the onset of constriction at faster growth rates. The possible molecular pathway, which is consistent with our and other published data, involves the formation of FtsZ bundles (doublets), which drive FtsA from a monomer and short arc form to an antiparallel filament form. FtsA antiparallel filament form is competent in the recruitment of FtsN, which activates the core divisome complex and starts the onset of constriction.

Although the existing data is consistent with the proposed model (Fig. 5a), alternative explanations cannot be ruled out. To validate the model in Fig. 5a further, the existence of FtsZ protofilament doublets and bundles needs a more thorough in vivo verification. Also, in vitro measurements assessing the role of FtsZ protofilaments on the assembly of FtsA antiparallel filaments would be valuable. Finally, the question also remains on how the core divisome complex, consisting of FtsIW, FtsBQL, and FtsK, is exactly linked to FtsA antiparallel filaments.

Methods

Bacterial strains

All *E. coli* strains used in the reported experiments are derivatives of K12 BW27783 obtained from the Yale Coli Genetic Stock Center (CGSC#: 12119). Information on all strains and plasmids are listed in Supplementary Tables 1 and 2, respectively. Oligonucleotide information is given in Supplementary Table 3.

For FtsZ and FtsN overexpression measurements, we constructed three strains: 1) the strain of interest (SOI) that overexpressed unlabeled gene of interest in addition to the native one, 2) the Reporter strain that expresses fluorescent fusion protein instead of the gene of interest from the same genomic locus, 3) the Reference strain that expresses fluorescent fusion to the gene of interest from its endogenous locus.

Strains for FtsZ overexpression measurements

Firstly, a plasmid pEXT22-FtsZ (pJM142) with unlabeled FtsZ under the control of an isopropyl-β-D-thiogalactoside (IPTG) inducible P_{tac} promoter was constructed. Briefly, FtsZ was amplified from plasmid JW0093[3] using primers PR200 and PR201. The Ribosome Binding Sequence (RBS, TAGAGAAAGAGGAGAAATACTAG) was introduced in part of the forward primer in front of the *ftsZ* sequence. The resulting insert (*xbaI_RBS_ftsZ_hindIII*) was cloned into vector pEXT22[59] using restriction enzymes *XbaI* and *HindIII*. The same approach was also used for the Reporter plasmid expressing *mNeonGreen* (*mNG*) instead of *ftsZ*. In this case, *mNG* was amplified from plasmid pJM21 (Männik lab) using primers PR202 and PR203. The resulting insert (*xbaI_RBS_mNG_hindIII*) was ligated into pEXT22 using restriction enzymes *XbaI* and *HindIII* and transformed into DH5α competent cells (Thermo Scientific). After verification by restriction analysis and DNA sequencing, the plasmids were transformed into the BW27783 strain, yielding strains JM237 (FtsZ expressing) and JM228 (mNG Reporter).

To obtain low-level FtsZ overexpression SOI (JM252) and corresponding Reporter mNG expressing strain (JM250), the DNA cassette of the *lacI*^{q}-p_{Tac}-*ftsZ-aph* from pEXT22-FtsZ was introduced into the λ-attachment (*attB*) site by *λ*-Red engineering[60]. For chromosome insertion, the *lacI*^{q}-p_{Tac}-*ftsZ-aph* cassette was amplified from plasmid pEXT22-FtsZ using primers (PR206/ PR207), each composed of a 42 (44)-bp sequence at the 5′ end homologous to the *attB* region. The resulting PCR product was treated with *DpnI* (NEB), gel purified using GeneJET Gel Extraction and DNA Cleanup Micro Kit (Thermo Scientific), and then electroporated into a JM217 strain containing pSIM5[60] that encodes λ-Red proteins. Kanamycin-resistant colonies were verified by using colony PCR with primers PR210 and PR211 (or PR212), followed by direct sequencing. The *lacI*^{q}-p_{Tac}-*ftsZ-aph* allele was then transduced from JM246 into BW27783 by P1 transduction to generate strain JM252. In parallel, the same procedures were conducted to make the Reporter strain expressing mNG from the *attB* locus. Finally, the *lacI*^{q}-p_{Tac}-*mNG-aph* allele was transduced from JM248 into BW27783 to generate strain JM250. The Reference strain (JM147) expresses endogenous FtsZmNG. The same Reference was also used in the above-described experiments with pEXT22-FtsZ. To construct a strain JM276 expressing the *lacI*^{q}-p_{Tac}-*ftsZmNG-aph* from the λ-attachment site, a similar approach to that described for the unlabeled FtsZ strain (JM252) was used, with the exception that the *ftsZmNG* sequence was amplified from the HE1 strain expressing endogenous FtsZ sandwich fusion to fluorescent mNG (FtsZmNG)[46]. The construct was recombineered to WT strain, resulting in strain JM261, and then transduced from JM261 into HE1, resulting in strain JM276. To obtain a strain JM275, a *lacI*^{q}-p_{Tac}-*ftsZ-aph* allele in the λ-attachment site from the JM252 strain was transduced into the HE1 strain.

Strains for FtsN overexpression measurements

For FtsN over-expression strains (JM200, JM230), a plasmid expressing Ypet-FtsN (JM200) and unlabeled FtsN (JM230) under the control of an IPTG inducible weakened P_{trc} promoter was constructed. *Ypet-ftsN* was amplified from the gDNA of the STK13 strain[11] using primers PR204 and PR205. The resulting insert (*ecoRI_RBS_ypet-ftsN_hindIII*) was cloned into vector pDSW210 (JM149) using restriction enzymes *EcoRI* and *HindIII*. For unlabeled FtsN expression, *ftsN* was amplified from plasmid pDSW210-Ypet-FtsN using primers PR213 and PR205. The resulting insert (*xmaI_ftsN_hindIII*) was cloned into pDSW210-Ypet-FtsN (JM230) using restriction enzymes *XmaI* and *HindIII*. Also, the Reporter strain expressing plasmid pDSW210-Ypet was constructed in a similar way. In this case, *ypet* was amplified from pDSW210-Ypet-FtsN using primers PR204 and PR214. The resulting insert (*ecoRI_RBS_ypet_hindIII*) was cloned into pDSW210-Ypet-FtsN (JM200) using restriction enzymes *EcoRI* and *HindIII*. To be able to compare expression levels of labeled and unlabeled FtsN strains, the same sequence, including RBS, was retained in front of the *ypet* sequence in pDSW210-Ypet (JM241), in front of *ftsN* expressed from pDSW210-FtsN (JM230), in front of *ypet-ftsN* expressed from pDSW210-Ypet-FtsN (JM200) as it is in upstream of native *ypet-ftsN* in strain STK13.

For low-level overexpression of FtsN and Ypet-FtsN, the DNA cassette sequences from respective plasmid constructs were inserted into the *attB* site by *λ*-Red engineering as described above for the *ftsZ* gene. Briefly, the *lacI*^{q}-p_{Trc}-*ftsN-bla* and *lacI*^{q}-p_{Trc}-*ypet-ftsN-bla* cassette was amplified from a template plasmid pJM230 or pJM200, respectively, using primers (PR208/ PR209) and electroporated into JM217 strain with pSIM5 plasmid. Ampicillin-resistant colonies were verified by colony PCR with primer pair PR210/PR211, followed by direct sequencing. In the final step, the resulting alleles were transferred to BW27783 genetic background by P1 transduction generating strains JM235 (inducible unlabeled FtsN at the *attB* site and endogenous mCherry-DnaN) and JM222 (inducible Ypet-FtsN at the *attB* site). Additionally, the *lacI*^{q}-p_{Trc}-*ypet-ftsN-bla* allele was transferred to the STK13 expressing endogenous Ypet-FtsN and mCherry-DnaN, resulting in the JM223 strain.

Strains for FtsA and FtsA* (FtsA^{R286W}) overexpression measurements

Plasmids expressing *ftsA* (pDSW210-ftsA, also known as pSEB306 +) and *ftsA** (pDSW210-ftsA*, also known as pSEB306*+) under an IPTG inducible promoter were transformed into BW27783 generating strains JM242 and JM243, respectively. The strain JM149 containing pDSW210-GFP expressed GFP under an IPTG inducible promoter and was used as the Reporter. These three plasmids were described previously[61]. These upregulation measurements lacked reference strain because of an absence of genomically integrated fully functional FtsA. Instead, Western blotting was used to determine the final $[FtsA]_{norm}$ for 100 μM IPTG induction[9,61] for both FtsA (2.39x) and FtsA* (2.43x) overexpression measurements. The corresponding calibration factor was also used to quantify the expression level of FtsA in low overexpression conditions (1.43x), where 30 μM IPTG induction was used.

For *E. coli* strain construction, the cells were grown in lysogeny broth (LB) and appropriate selective antibiotics.

The new bacterial strains first described in this work are available from the corresponding author upon reasonable request.

Growth media and growth conditions

For time-lapse imaging in microfluidic devices, the cells were cultured in M9 minimal media supplemented with 2 mM magnesium sulfate, 0.5% glucose as the carbon source, 0.5% casamino acids (CAS), and 1x trace metals mixture (Tre) at 28 °C. In measurement where alanine was used as a carbon source, M9 minimal media was supplemented with 0.5% alanine (Millipore Sigma, MO) and 1x Tre. When appropriate, the medium was supplemented with 100 μg/ml ampicillin (Amp) or 40 μg/ml kanamycin (Kan). Amp and Kan concentrations were reduced to 20 μg/ml when cells carried *bla* or *aph* integrated into the chromosome. For induction, IPTG (30 μM, 100 μM, 500 μM, or 1 mM) was included in the media.

Cell preparation and culture in microfluidic devices

The strains were streaked on M9 minimal media agar plates supplemented with magnesium sulfate, glucose, CAS, Tre, and appropriate selective antibiotics. For the microscopy experiment, a colony from a fresh plate was inoculated into 3 ml of M9 minimal salt media supplemented with carbon source and additives described above. 40 μg/ml of Kan was added to grow strains JM147, JM228, and JM237.

100 μg/ml of Amp to grow strains JM149, JM230, JM241, JM242 and JM243. The cells were grown to an OD_{600} of ~0.1 in a liquid medium and then concentrated ~100x by centrifugation in the presence of 0.075 μg/ml of BSA (Bovine Serum Albumin; Millipore Sigma, MO) to minimize clumping of the cells. For the overexpression experiments, three strains - strain of interest (SOI), Reporter, and Reference were prepared the same way, mixed thoroughly in the Eppendorf tube before loading to PDMS (polydimethylsiloxane) - based mother machine microfluidic device. The latter were prepared following a previously described procedure[62]. The concentrated mix of three strains was pipetted onto the main flow channel of the mother machine device to populate the dead-end channels of the device for one hour. Next, a 10-ml syringe (Becton Dickinson, Fisher Scientific) was prepared with fresh M9 growth medium with the carbon source, additives, BSA (0.075 μg/ml), and appropriate antibiotics when needed and mounted on NE-1000 Syringe Pump (New Era Pump Systems, NY). The tubing was connected to the device, and the flow of fresh M9 medium started and was kept at 6 μl/min during the entire experiment. The cells were left to grow in channels overnight (at least 14 hr) to ensure steady-state growth. Only the cells that are daughters of the mother cell (the cell at the end of the channel) will remain in the channel after this period. This procedure thus ensures that cells in each channel are from only a single strain when the imaging starts. The next morning, two 10-ml syringes were prepared with fresh growth medium (to one syringe inducer IPTG was added) and mounted on separate NE-1000 Syringe Pumps. A T-junction was formed with three pieces of tubing and a T-connector. Before applying IPTG to induce the expression of the gene of interest (*ftsZ*, *ftsN*, *ftsA* or *ftsA**) and the Reporter (*mNeonGreen*, *Ypet* or *Gfp*) from the extra copy at the *attB* site (or from the plasmid), cells were imaged in regular M9 media. After 10 h of imaging, the first pump with the regular media was turned off, and the second syringe pump containing regular media with IPTG was turned on without interrupting imaging using a custom-made LabVIEW program. Altogether, cells were imaged for 22-26 hrs. For a list of all SOI, Reference, and Reporter strains and inducer IPTG concentrations used in experiments see Supplementary Table 4.

Fluorescence microscopy

A Nikon Ti-E inverted fluorescence microscope (Nikon Instruments, Japan) with a 100X NA 1.40 oil immersion phase-contrast objective (Nikon Instruments, Japan) was used to image the bacteria. Images were captured on an iXon DU897 EMCCD camera (Andor Technology, Ireland) and recorded using NIS-Elements software (Nikon Instruments, Japan). Fluorophores were excited by a 200 W Hg lamp through ND4 and ND8 neutral density filters. Chroma 41001 and 41004 filter cubes (Chroma Technology Corp., VT) were used to record mNeonGreen/Ypet and mCherry images, respectively. A motorized stage (Prior Scientific Inc., MA) and a Nikon Perfect Focus® system were utilized throughout time-lapse imaging. Images in M9 glucose-cas were obtained at 3 min frame rate. The typical exposure times were 400 ms at an EM gain of 200 for mNeonGreen/Ypet and 400 ms without EM gain for the phase images. The mCherry signal was recorded before the FtsN upregulation experiment to distinguish between strains JM235, STK13, and JM222 (expose time 250 ms at EM gain 200). mCherry signal was not recorded during the FtsN upregulation measurements.

Image analysis

MATLAB, along with the Image Analysis Toolbox and DipImage Toolbox (http://www.diplib.org/) and Python 3.11.4 with torch and torchvision packages (https://pytorch.org/) were used for image analysis. In all analyses of time-lapse recordings, corrections to subpixel shifts between different frames were applied first. These shifts were determined by correlating phase-contrast images in adjacent frames. Individual channel images were then cropped. A convolution neural network, referred to as the Omnipose[63], was used for cell segmentation. The network was first trained on images obtained from the experimental setup used in this work. The resulting cell masks were then assembled into cell lineages using a custom MATLAB script. The same script also calculated the cell lengths based on these cell masks[64].

Fluorescence induction model to determine protein concentrations

To determine the induced protein concentrations, the total fluorescence intensity from fluorescent fusion proteins of the Reporter and the Reference strains were determined as a function of time from cell images. The same fluorescent fusion (either mNeonGreen or Ypet) was used in both strains. To calculate the total intensity, the pixel values from 11 pixels (1.2 μm) wide band around the cell centerline were summed. This band is slightly wider than the cell (about 0.8 μm). The intensity was then normalized per pixel value. The same normalized intensity was also calculated for the unlabeled SOI, and the average value from the cell population from SOI was subtracted from the normalized intensities from the Reporter and the Reference strain populations at each binned timepoint. The per-pixel normalized and background-corrected intensity from the Reporter strain was then divided by the per-pixel normalized and background-corrected intensity from the Reference strain. Since the fluorescence from the Reference did not significantly vary in time, a single global value of the per pixel normalized and background-corrected intensity from the Reference strain was used for division. The resulting quantity is referred to as the Normalized Reporter Signal and is plotted in Figs. 1, 2a, 3a, 3d, 4a and 4g in the main Text. However, this quantity reflects the induced concentration of the mature fluorescent fusion protein in the Reporter strain, not the concentration of the total fluorescent fusion proteins in the Reporter. To determine this total concentration, we fitted the data in these plots to a previously described model[7]. The model has an analytic solution for the normalized mature protein concentration in the Reporter as a function of time:

$$[X]_{norm,m}(t) = [X]_{norm,m0} + \Delta[X]_{norm,m}\left[1 - e^{-\mu(t-t_0)}\left\{1 + \frac{\mu}{k_m}\left(1 - e^{-k_m(t-t_0)}\right)\right\}\right] t > t_0,$$

where t_0 is the time of the induction, $[X]_{norm,m0}$ is the concentration before induction including the leakage, $\Delta[X]_{norm,m}$ is the increase of the normalized concentration as a result of induction, μ is the population-average growth rate, and k_m is the maturation rate of the fluorescent protein. X stands for FtsZ and FtsN. The solution before induction is $[X]_{norm,m}(t) = [X]_{norm,m0}$ $(t<t_0)$. The maturation rate in these growth conditions (glucose-CAS medium in 28 °C) for mNeonGreen was determined to be $k_m = 0.029$ min^{-1} previously[7]. For Ypet we used the same chloramphenicol treatment procedure as in[7,65] to find $k_m = 0.049$ min^{-1}. We calculated the population average growth rate as $\mu = \ln(2)/T_d$ using T_d value before induction. The above expression for $[X]_{norm,m}(t)$ was fitted to the Normalized Reporter Signal using MATLAB *fminsearch* function treating μ as a constant. The fittings are plotted for different proteins of interest in Figs. 1, 2a, 3a, d, 4a, g.

The fit yielded parameters t_0, $[X]_{norm,m0}$ and $\Delta[X]_{norm,m}$ (the fitting line is shown by blue lines in the main text figures). Based on these parameters we calculated the total fluorophore concentration in the Reporter cells:

$$[X]_{norm}(t) = [X]_{norm,0} + \Delta[X]_{norm}\left(1 - e^{-\mu(t-t_0)}\right) t > t_0.$$

Note that $[X]_{norm,0} = [X]_{norm,m0}$ and $\Delta[X]_{norm} = \Delta[X]_{norm,m}$ if both are normalized by the corresponding WT concentrations, that is, $[X]_{norm,m}$ is normalized by the mature fluorophore concentration in the Reference strain and $[X]_{norm}$ is normalized by the total protein of interest concentration in WT cells. In this normalization,

$[X]_{norm} = 1.0x$ is the concentration of protein in WT cells. We use throughout the text a notion the final $[X]_{norm}$. The latter is the final steady state value after the induction and based on the above equation is given by $[X]_{norm} = [X]_{norm,0} + \Delta[X]_{norm}$. According to the equation for $[X]_{norm}(t)$, the time dependence in the total fluorophore/protein of interest concentration in the cells is solely determined by the growth rate μ. Fitting is still needed to determine accurately t_0, $[X]_{norm,0}$ and $\Delta[X]_{norm}$.

Since the Reporter expressed the fluorescent reporter exactly from the same locus (the same promoter and ribosome binding site), the total fluorescent protein concentration can be taken to be equal to the total protein of interest concentration in the cells. This holds under the assumption that the protein of interest is not degraded. While FtsZ has significant degradation at lower growth rates by ClpXP protease, the degradation was undetectable in glucose-CAS medium[7], which is used in this work.

There is no reference strain in FtsA and FtsA* upregulation measurements due to the lack of sufficiently functional FtsA fluorescent fusion that can replace the native *ftsA*. For FtsA and FtsA* measurements, the final $[FtsA]_{norm}$ was determined based on Western blotting for IPTG induction level of 100 μM. The fluorescent microscopy measurements still had the Reporter strain. The signal from the Reporter strain determined $[FtsA]_{norm,0}$. For the FtsA upregulation measurements at [IPTG] of 30 μM, the same conversion factor for fluorescent signal was used as in upregulation measurements at [IPTG] of 100 μM.

The values for $[X]_{norm,0}$ ($=[X]_{norm,m0}$), $\Delta[X]_{norm}$ ($=\Delta[X]_{norm,m}$), t_0 and the final $[X]_{norm}$ (= the final $[X]_{norm,m}$) for each measurement are listed in Supplementary Table 4.

Determining the timing for the onset of constriction

The signal from the phase contrast images was used to determine the onset of constriction. The intensity line profiles along the long axes of the cell were averaged first, as described before[9]. The program then searched for the local maximum in this profile near the cell middle. The constriction timing was chosen as the earliest frame when the minimum was present, with an additional condition that this minimum persisted for at least two out of three measurement frames until the cell divided.

Determining the Z-ring and N-ring-related parameters

The timings for the Z-ring formation were determined using fully automated analysis. To this end, the intensity line profiles from each frame of FtsZmNG signal were fitted to a Gaussian. If the width of the fitted peak (FWHM) of the Gaussian was between 200 and 1000 nm, and the peak was not more than 10% off from the cell center in terms of cell length, then this fitting qualified as an accumulation. The timing for the first qualifying accumulation in the cell cycle determined timing $Tz,1$. To determine the timing for the persistent Z-ring (Tz,per) the accumulations had to be present from this point onward until the end of the cell cycle, but single frame misses were allowed. To find the number of FtsZ in the Z-ring (as in Fig. 2i, and Supplementary Fig. 11a-d), the integrated intensity from the Gaussian was calculated. Although the number of FtsZ in the Z-ring is in arbitrary units, these units are the same as those used for the total number of FtsZ. To find the excess number of FtsZ (as in Supplementary Fig. 11e–h and Fig. 16c) and FtsN molecules in the cell middle (as in Fig. 16a), integrated fluorescent intensity form a 0.75 μm wide band (7 pixels wide) centered at the midcell was calculated. From this integrated intensity, a cell background intensity was subtracted. The background intensity for subtraction was also integrated from a 0.75 μm wide band (7 pixels wide). The latter band was centered at the ¼ position from the old pole of the cell. The non-fitting-based and fitting-based methods gave comparable results when a detectable Z-ring was present.

Western blot analysis

To independently verify the final normalized concentrations from the fluorescence-based measurements (the final $[X]_{norm}$), we also determined these concentrations by Western blotting (Supplementary Fig. 1). For the Western blotting of FtsZ, overnight cultures of JM252, JM147 and BW27783 cells were diluted to an OD600 of 0.005 in fresh M9 glucose-CAS medium and grown at 28 °C for about 5 hrs until reaching an OD600 of 0.04-0.05. The cultures were then diluted back to an OD600 of 0.005 in M9 glucose-CAS and divided into triplicate sets. To one set of JM252 cells, 500 μM of IPTG (Millipore Sigma, MO) was added. Cells grown in the glucose-CAS medium were collected after 7 h of induction, corresponding to an OD600 of 0.4-0.5 as determined at the time of collection. The 7-hour time period was chosen based on the procedure used in the microfluidic experiments, during which cells reached a stable expression of FtsZ from the *attB* site. The collected cells were pelleted, resuspended in lysis buffer (50 mM Tris pH8, 300 mM NaCl, 10 mM MgCl2, 1 mM EDTA) and stored at −80 °C. For lysis, cells were thawed and incubated with lysozyme (10 mg/ml, MP Biomedicals) and DNase (1 mg/ml, ThermoFisher Scientific) in the presence of Pierce Protease Inhibitor mix (ThermoFisher Scientific). The resulting extract was mixed with SDS sample buffer (LI-COR Biosciences) according to the optical density (OD) of the collected cells, boiled for 10 min, and separated by SDS-PAGE in a Mini PROTEAN Tetra Cell (Bio-Rad) using precast 12% polyacrylamide gels (Bio-Rad). Proteins were transferred to a low-fluorescence PVDF membrane (ThermoFisher Scientific) using a Bio-Rad Mini Trans-Blot Cell. The membrane was blocked with Odyssey® blocking buffer (LI-COR Biosciences) according to the manufacturer's protocol. Primary antibodies (anti-FtsZ at final concentration 1:2000, Agrisera AB, AS10 715, Lot 1608) were diluted in blocking buffer and incubated overnight at 4 °C. The secondary donkey anti-rabbit IRDye 680RD antibodies (LI-COR Biosciences, cat# 926-68073, Lot C80918-07) were used at the dilution of 1:15,000 for 45 min at room temperature, followed by three washes (TBST, 15 min each). Images of the near-infrared fluorescent signal were acquired using an Odyssey scanner (LI-COR Biosciences).

To compare the level of native FtsN, uninduced and induced extra FtsN from the *attB* site, BW27783 and JM235 strains were cultured in M9 glucose-CAS medium as described above for the FtsZ Western blot cultures. To induce expression of FtsN from the *attB* site (JM235), 1 mM of IPTG (Millipore Sigma, MO) was added to a set of JM235 cells. The cells were collected after 7 h, corresponding to an OD600 of 0.4-0.55.

The collected cells were resuspended in an SDS sample buffer, the amount of which was adjusted according to the cells' OD, and boiled for 10 min before being loaded on the SDS-PAGE gel for analysis. Western blotting and detection of FtsN were performed as described above, except for the primary antibodies. For FtsN detection, 1:350 dilution of the anti-FtsN antiserum (UK43; Lutkenhaus lab) in Odyssey blocking buffer was used.

The Western blot analysis for FtsA is from an earlier work[9] as the same extra copy construct and induction was used in measurements here. Western blotting and detection of FtsA were performed as described above, except for the primary antibodies for which an anti-FtsA serum was used at a final concentration of 1:750 (UK54, Lutkenhaus lab).

To analyze the Western blot images, we first acquired intensity line profiles from each lane using ImageJ. The line profiles had the same width for a given image and encompassed approximately the entire band. To obtain the integrated intensities from the bands, we fitted the line profiles to one or two Gaussians with a background term in Origin Pro 2016. Two Gaussians were used to fit the FtsZ and FtsA signals where spurious bands were close to the band from the protein of interest (POI). The three measurements were then averaged and std calculated. The signal was then further normalized using the value obtained from the WT strain. For the final variance of the POI, the

squares of the relative errors of POI and WT strains were summed. The error bar for POI is the square root of this final variance.

To further verify that the cell numbers contributing to each lane were the same, we also acquired reference bands from each Western blot (indicated by an asterisk in Supplementary Fig. 1). We chose the reference bands as high molecular weight bands, which could not have originated from the POI. The integrated intensities from the reference band were acquired as described above for the POI bands. We also quantified the protein abundances by dividing the signal from each lane from POI to that of the Reference. The resulting abundances were effectively the same as when the reference bands were not used, but error bars were somewhat higher.

Western blot analysis shows about 15% lower overexpression levels for FtsN and 27% lower for FtsZ than the fluorescence-based measurements (Supplementary Table 5). This could be due to the degradation of FtsZ and FtsN in the cells, unlike the fluorescent reporter, which is not expected to be degraded. Indeed, for FtsZ 10-50% degradation during the cell cycle has been reported before[7,66]. The latter number depends on the growth rate of the cells being higher at lower growth rates[63]. On the other hand, the relative error for the Western blotting results is about 30% for the final $[\mathrm{FtsZ}]_{norm}$ and 25% for the final $[\mathrm{FtsN}]_{norm}$ (Supplementary Table 5). Accounting for these errors, the difference between the Western blot and fluorescence-based measurements is neglected.

Modeling

We compare the experimental data to the concurrent processes model where the slowest of the two limiting processes controls the start of septum formation[36] rather than cell division[41,42]. Based on an earlier report[67], we assume that the cell size (length) grows exponentially with rate λ_{bf} before the septum formation starts. The cells grow with a different growth rate, λ_{af}, after the onset of constriction. λ_{bf} and λ_{af} is sampled from a normal distribution with the mean value determined from experimental data as $\langle\lambda_{bf}\rangle = (1/\langle Tc\rangle)\ln(\langle \mathrm{Lc}\rangle/\langle \mathrm{Lb}\rangle) = 0.0087\ \mathrm{min}^{-1}$ and $\langle\lambda_{af}\rangle = (1/\langle Td - Tc\rangle)\ln(\langle \mathrm{Ld}\rangle/\langle \mathrm{Lc}\rangle) = 0.0126\ \mathrm{min}^{-1}$. $\langle\ \rangle$ denotes the mean and the experimental data is from the 1.96x FtsZ overexpression experiment (Fig. 2a-c). The coefficient of variation (CV) is fixed to be 0.2 consistent with the CV observed for growth rate. The two limiting processes are: 1. Inhibitory process related to DNA replication that blocks the onset of constriction for a time Tic that is measured from the initiation of DNA replication. Tic is drawn from a normal distribution with mean $\langle Tic\rangle$ and CV$\approx$ 0.2 which is consistent with CV values of time variables. 2. FtsZ accumulation to a threshold amount. The amount of FtsZ (number) increases at a rate proportional to the cell size i.e., $\frac{dN}{dt} = sL$. The production rate of FtsZ, s, is fixed at the start of each cell cycle and is assumed to be normally distributed with mean $\langle s\rangle = 1{+}s_i$ (in units of $\langle\lambda_{bf}\rangle$) and CV $\approx$ 0.2. s_i is the leakage in FtsZ production before FtsZ is overexpressed. The upshift in FtsZ production is modeled as a step function with the mean production rate increasing from $1{+}s_i$ to $1{+}s_i{+}f$ instantaneously. The factor f is determined using the steady-state normalized concentration of fluorescent protein in the Reporter strain. FtsZ accumulates to a threshold value drawn from a normal distribution with a mean N^* and CV = 0.2. The values of the two model parameters $\langle Tic\rangle$ and N^* are determined to be such that the average lengths at constriction before and after 1.96x FtsZ overexpression match between simulations and experiments. For a range of values of N^* and $\langle Tic\rangle$, we find the value of the cost function

$$C = \sqrt{\left(\frac{Lc_{bf,sim}}{Lc_{bf,\,\mathrm{exp}}} - 1\right)^2 + \left(\frac{Lc_{af,sim}}{Lc_{af,\,\mathrm{exp}}} - 1\right)^2}$$

where $Lc_{bf,sim}$ and $Lc_{af,sim}$ are the steady-state values of Lc before and after overexpression obtained from simulations, respectively. $Lc_{bf,\,\mathrm{exp}}$ and $Lc_{af,\,\mathrm{exp}}$ are the steady state values of Lc obtained from experiments. The cost function has a minimum for $\langle Tic\rangle$ = 75.6 min and N^* = 286 (Supplementary Fig. 21).

To simulate the DNA replication cycle and constriction processes, we use previously specified models. The initiation of DNA replication is determined by an adder per origin model[31,34] where cells added a constant length increment per origin Δ_{ii} from one initiation of DNA replication to the next. Δ_{ii} is drawn from a normal distribution with mean $\langle\Delta_{ii}\rangle = 0.6\ \mu m$ and CV = 0.1 determined using experimental data in previous studies[11]. The cell division happens after a time ΔTs from the onset of constriction[68]. ΔTs is normally distributed with a mean determined from experiments and is equal to $\langle Td - Tc\rangle$ = 18.3 min and CV is fixed to be 0.2. The value of ΔTs changes slightly (by 1.5 min) after FtsZ overexpression (Supplementary Fig. 6). This is included as a step function in $\langle\Delta Ts\rangle$ value. The cell divides on average symmetrically but with a noise in division ratio. The standard deviation in the division ratio is 0.03[69].

The upshift in FtsZ production is obtained by monitoring the concentration of a mature reporter protein. The reporter protein exists in two states - a mature state which is observed and an unmatured state. The protein goes from an unmatured to a mature state at a rate $k_m = 0.029\ \mathrm{min}^{-1}$ in FtsZ upregulation measurements. The total amount of the reporter protein is a proxy for the FtsZ amount. In the simulations, the amount of mature protein (N_m) at each time step is $\frac{dN_m}{dt} = k_m(N - N_m)$, where is $N - N_m$ is the amount of immature protein. Upon division, each daughter cell gets exactly half of the matured and total proteins.

We compared the results above to another model of cell division (Supplementary Fig. 12) where the two limiting processes controlling it were: 1. FtsZ accumulation to a threshold (like in the previous model) and 2. another cell division-related protein accumulating to a threshold amount (instead of the replication-related process being limiting). The threshold amount was chosen by minimizing the cost function C above, keeping the rest of the parameters (including the FtsZ threshold N^*) fixed. We assumed the same relative noise level in the threshold values for the other cell division-related protein as for FtsZ (CV = 0.2). The minimization of the cost function resulted in the threshold of 251 for the other division-related protein.

Comparing the concurrent processes model to FtsA upregulation measurements, we assumed in the model, based on Fig. 4f, that the increase in FtsA concentration when $[\mathrm{FtsA}]_{\mathrm{norm}}$>1.6x leads to a linear increase in FtsZ threshold numbers, that is $N^* = N_0^*(1+\alpha([\mathrm{FtsA}]_{\mathrm{norm}} - 1.6\mathrm{x})/[\mathrm{FtsA}]_{\mathrm{norm,\,final}})$ for $[\mathrm{FtsA}]_{\mathrm{norm}}$>1.6x and a constant value, $N = N_0^*$, for $[\mathrm{FtsA}]_{\mathrm{norm}} \le 1.6\mathrm{x}$. Here, $N_0^* = 286$ as used in simulations of FtsZ upregulation. We adjust the coefficient of proportionality, α, manually to 0.07 (7%) to fit the Lc vs time curve in Fig. 4d. All other parameters of the model are kept the same as in Fig. 2. Instead of directly simulating the increase in $[\mathrm{FtsA}]_{\mathrm{norm}}$, we used the formula from the fluorescence induction model $[\mathrm{FtsA}]_{\mathrm{norm}} = 1 + ([\mathrm{FtsA}]_{\mathrm{norm,\,final}} - 1)(1 - \exp(-\mu t))$ as the latter approach matches well the corresponding average curve of the stochastic simulations.

Reporting summary

Further information on research design is available in the Nature Portfolio Reporting Summary linked to this article.

Data availability

The data generated in this study are provided in the Source Data file. Source data are provided with this paper.

Code availability

The custom MATLAB scripts used to analyze the data are available from Zenodo (https://doi.org/10.5281/zenodo.13988793)[64]. The codes to create concurrent processes modeling data are available also from Zenodo (https://doi.org/10.5281/zenodo.13987797)[70].

References

1. Cameron, T. A. & Margolin, W. Insights into the assembly and regulation of the bacterial divisome. *Nat. Rev. Microbiol* **22**, 33–45 (2024).
2. Du, S. S. & Lutkenhaus, J. At the heart of bacterial cytokinesis: the Z ring. *Trends Microbiol.* **27**, 781–791 (2019).
3. Yang, X. X. et al. GTPase activity-coupled treadmilling of the bacterial tubulin FtsZ organizes septal cell wall synthesis. *Science* **355**, 744–747 (2017).
4. Bisson, A. W. et al. Treadmilling by FtsZ filaments drives peptidoglycan synthesis and bacterial cell division. *Science* **355**, 739–743 (2017).
5. Yao, Q. et al. Short FtsZ filaments can drive asymmetric cell envelope constriction at the onset of bacterial cytokinesis. *EMBO J.* **36**, 1577–1589 (2017).
6. Holden, S. J. et al. High throughput 3D super-resolution microscopy reveals *Caulobacter crescentus* in vivo Z-ring organization. *Proc. Natl Acad. Sci. USA.* **111**, 4566–4571 (2014).
7. Männik, J., Walker, B. E. & Männik, J. Cell cycle-dependent regulation of FtsZ in *Escherichia coli* in slow growth conditions. *Mol. Microbiol.* **110**, 1030–1044 (2018).
8. Aarsman, M. E. G. et al. Maturation of the *Escherichia coli* divisome occurs in two steps. *Mol. Microbiol.* **55**, 1631–1645 (2005).
9. Männik, J., Pichoff, S., Lutkenhaus, J. & Männik, J. Cell cycle-dependent recruitment of FtsN to the divisome in *Escherichia coli*. *mBio* **13**, e0201722 (2022).
10. Harris, L. K. & Theriot, J. A. Relative rates of surface and volume synthesis set bacterial cell size. *Cell* **165**, 1479–1492 (2016).
11. Tiruvadi-Krishnan, S. et al. Coupling between DNA replication, segregation, and the onset of constriction in *Escherichia coli*. *Cell Rep.* **38**, 110539 (2022).
12. de Boer, P. A. J. Advances in understanding *E. coli* cell fission. *Curr. Opin. Microbiol.* **13**, 730–737 (2010).
13. Gerding, M. A. et al. Self-enhanced accumulation of FtsN at division sites and roles for other proteins with a SPOR domain (DamX, DedD, and RlpA) in *Escherichia coli* cell constriction. *J. Bacteriol.* **191**, 7383–7401 (2009).
14. Liu, B., Persons, L., Lee, L. & de Boer, P. A. J. Roles for both FtsA and the FtsBLQ subcomplex in FtsN-stimulated cell constriction in *Escherichia coli*. *Mol. Microbiol.* **95**, 945–970 (2015).
15. Weiss, D. S. Last but not least: new insights into how FtsN triggers constriction during *Escherichia coli* cell division. *Mol. Microbiol.* **95**, 903–909 (2015).
16. McCausland, J. W. et al. Treadmilling FtsZ polymers drive the directional movement of sPG-synthesis enzymes via a Brownian ratchet mechanism. *Nat. Commun.* **12**, 609 (2021).
17. Lutkenhaus, J. FtsN-trigger for septation. *J. Bacteriol.* **191**, 7381–7382 (2009).
18. Daley, D. O., Skoglund, U. & Soderstrom, B. FtsZ does not initiate membrane constriction at the onset of division. *Sci. Rep.* **6**, 33138 (2016).
19. Lyu, Z. et al. FtsN maintains active septal cell wall synthesis by forming a processive complex with the septum-specific peptidoglycan synthases in *E. coli*. *Nat. Commun.* **13**, 5751 (2022).
20. Nierhaus, T. et al. Bacterial divisome protein FtsA forms curved antiparallel double filaments when binding to FtsN. *Nat. Microbiol.* **7**, 1686–1701 (2022).
21. Britton, B. M. et al. Conformational changes in the essential *E. coli* septal cell wall synthesis complex suggest an activation mechanism. *Nat. Commun.* **14**, 4585 (2023).
22. Taguchi, A. et al. FtsW is a peptidoglycan polymerase that is functional only in complex with its cognate penicillin-binding protein. *Nat. Microbiol.* **4**, 587–594 (2019).
23. Yang, X. et al. A two-track model for the spatiotemporal coordination of bacterial septal cell wall synthesis revealed by single-molecule imaging of FtsW. *Nat. Microbiol* **6**, 584–593 (2021).
24. Marmont, L. S. & Bernhardt, T. G. A conserved subcomplex within the bacterial cytokinetic ring activates cell wall synthesis by the FtsW-FtsI synthase. *Proc. Natl Acad. Sci. USA.* **117**, 23879–23885 (2020).
25. Baranova, N. et al. Diffusion and capture permits dynamic coupling between treadmilling FtsZ filaments and cell division proteins. *Nat. Microbiol* **5**, 407–417 (2020).
26. Pichoff, S., Shen, B., Sullivan, B. & Lutkenhaus, J. FtsA mutants impaired for self-interaction bypass ZipA suggesting a model in which FtsA's self-interaction competes with its ability to recruit downstream division proteins. *Mol. Microbiol.* **83**, 151–167 (2012).
27. Radler, P. et al. In vitro reconstitution of *Escherichia coli* divisome activation. *Nat. Commun.* **13**, 2635 (2022).
28. Wagstaff, J. & Lowe, J. Prokaryotic cytoskeletons: protein filaments organizing small cells. *Nat. Rev. Microbiol.* **16**, 187–201 (2018).
29. Schoenemann, K. M. et al. Gain-of-function variants of FtsA form diverse oligomeric structures on lipids and enhance FtsZ protofilament bundling. *Mol. Microbiol* **109**, 676–693 (2018).
30. Krupka, M. et al. *Escherichia coli* FtsA forms lipid-bound minirings that antagonize lateral interactions between FtsZ protofilaments. *Nat. Commun.* **8**, 1–12 (2017).
31. Amir, A. Cell size regulation in bacteria. *Phys. Rev. Lett.* **112**, 208102 (2014).
32. Campos, M. et al. A constant size extension drives bacterial cell size homeostasis. *Cell* **159**, 1433–1446 (2014).
33. Taheri-Araghi, S. et al. Cell-size control and homeostasis in bacteria. *Curr. Biol.* **25**, 385–391 (2015).
34. Ho, P.-Y. & Amir, A. Simultaneous regulation of cell size and chromosome replication in bacteria. *Front. Microbiol.* **6**, 662 (2015).
35. Si, F. W. et al. Mechanistic origin of cell-size control and homeostasis in bacteria. *Curr. Biol.* **29**, 1–11 (2019).
36. Kar, P., Tiruvadi-Krishnan, S., Männik, J., Männik, J. & Amir, A. Using conditional independence tests to elucidate causal links in cell cycle regulation in *Escherichia coli*. *Proc. Natl Acad. Sci. USA* **120**, 110539 (2023).
37. Cooper, S. & Helmstetter, C. E. Chromosome replication and division cycle of *Escherichia coli* B/r. *J. Mol. Biol.* **31**, 519–540 (1968).
38. Wallden, M., Fange, D., Lundius, E. G., Baltekin, O. & Elf, J. The synchronization of replication and division cycles in individual *E. coli cells Cell* **166**, 729–739 (2016).
39. Witz, G., van Nimwegen, E. & Julou, T. Initiation of chromosome replication controls both division and replication cycles in *E. coli* through a double-adder mechanism. *Elife* **8**, 48063 (2019).
40. Bernander, R. & Nordstrom, K. Chromosome replication does not trigger. *Cell Div. Escherichia coli. Cell* **60**, 365–374 (1990).
41. Micali, G., Grilli, J., Osella, M. & Lagomarsino, M. C. Concurrent processes set *E. coli* cell division. *Sci. Adv.* **4**, aau3324 (2018).
42. Micali, G., Grilli, J., Marchi, J., Osella, M. & Lagomarsino, M. C. Dissecting the control mechanisms for DNA replication and cell division in *E. coli*. *Cell Rep.* **25**, 761–771 (2018).
43. Boye, E. & Nordstrom, K. Coupling the cell cycle to cell growth. *EMBO Rep.* **4**, 757–760 (2003).
44. Ward, J. E. Jr. & Lutkenhaus, J. Overproduction of FtsZ induces mini. *Cell Form. E. coli. Cell* **42**, 941–949 (1985).
45. Wang, H. C. & Gayda, R. C. High-level expression of the FtsA protein inhibits cell septation in *Escherichia coli* K-12. *J. Bacteriol.* **172**, 4736–4740 (1990).
46. Moore, D. A., Whatley, Z. N., Joshi, C. P., Osawa, M. & Erickson, H. P. Probing for binding regions of the FtsZ protein surface through site-directed insertions: discovery of fully functional FtsZ-fluorescent proteins. *J. Bacteriol.* **199**, https://doi.org/10.1128/JB.00553-16 (2017).
47. Walker, B. E., Männik, J. & Männik, J. Transient membrane-linked FtsZ assemblies precede Z-ring formation in *Escherichia coli*. *Curr. Biol.* **30**, 499–508 (2020).

48. Du, S. S., Pichoff, S. & Lutkenhaus, J. FtsEX acts on FtsA to regulate divisome assembly and activity. *Proc. Natl Acad. Sci. USA* **113**, E5052–E5061 (2016).
49. Mueller, E. A., Westfall, C. S. & Levin, P. A. pH-dependent activation of cytokinesis modulates Escherichia coli cell size. *PLoS Genet* **16**, e1008685 (2020).
50. Haeusser, D. P. & Margolin, W. Splitsville: structural and functional insights into the dynamic bacterial Z ring. *Nat. Rev. Microbiol.* **14**, 305–319 (2016).
51. Dai, K. & Lutkenhaus, J. The proper ratio of FtsZ to FtsA is required for cell-division to occur in *Escherichia coli*. *J. Bacteriol.* **174**, 6145–6151 (1992).
52. Geissler, B., Elraheb, D. & Margolin, W. A gain-of-function mutation in *ftsA* bypasses the requirement for the essential cell division gene zipA in *Escherichia coli*. *Proc. Natl Acad. Sci. USA.* **100**, 4197–4202 (2003).
53. Bi, E. & Lutkenhaus, J. FtsZ regulates frequency of cell division in Escherichia coli. *J. Bacteriol.* **172**, 2765–2768 (1990).
54. Corbin, L. C. & Erickson, H. P. A unified model for treadmilling and nucleation of single-stranded FtsZ protofilaments. *Biophys. J.* **119**, 792–805 (2020).
55. Erickson, H. P., Anderson, D. E. & Osawa, M. FtsZ in bacterial cytokinesis: cytoskeleton and force generator all in one. *Microbiol. Mol. Biol. Rev.* **74**, 504–528 (2010).
56. Szwedziak, P., Wang, Q., Bharat, T. A. M., Tsim, M. & Lowe, J. Architecture of the ring formed by the tubulin homologue FtsZ in bacterial cell division. *Elife* **3**, e04601 (2014).
57. Morrison, J. J., Conti, J. & Camberg, J. L. Assembly and architecture of Escherichia coli divisome proteins FtsA and FtsZ. *J. Biol. Chem.* **298**, 101663 (2022).
58. Park, K. T., Pichoff, S., Du, S. & Lutkenhaus, J. FtsA acts through FtsW to promote cell wall synthesis during cell division in *Escherichia coli*. *Proc Natl Acad Sci USA* **118**, https://doi.org/10.1073/pnas.2107210118 (2021).
59. Dykxhoorn, D. M., St Pierre, R. & Linn, T. A set of compatible tac promoter expression vectors. *Gene* **177**, 133–136 (1996).
60. Datta, S., Costantino, N. & Court, D. L. A set of recombineering plasmids for gram-negative bacteria. *Gene* **379**, 109–115 (2006).
61. Pichoff, S. & Lutkenhaus, J. Tethering the Z ring to the membrane through a conserved membrane targeting sequence in FtsA. *Mol. Microbiol.* **55**, 1722–1734 (2005).
62. Yang, D., Jennings, A. D., Borrego, E., Retterer, S. T. & Männik, J. Analysis of factors limiting bacterial growth in PDMS mother machine devices. *Front. Microbiol.* **9**, 871 (2018).
63. Cutler, K. J. et al. Omnipose: a high-precision morphology-independent solution for bacterial cell segmentation. *Nat. Methods* **19**, 1438–1448 (2022).
64. Mannik, J. Data analysis codes for: "Determining the rate-limiting processes for cell division in *Escherichia coli*", *Zenodo*, https://doi.org/10.5281/zenodo.13988793 (2024).
65. Balleza, E., Kim, J. M. & Cluzel, P. Systematic characterization of maturation time of fluorescent proteins in living cells. *Nat. Methods* **15**, 47–51 (2018).
66. Camberg, J. L., Hoskins, J. R. & Wickner, S. ClpXP protease degrades the cytoskeletal protein, FtsZ, and modulates FtsZ polymer dynamics. *Proc. Natl Acad. Sci. USA.* **106**, 10614–10619 (2009).
67. Kar, P., Tiruvadi-Krishnan, S., Männik, J., Männik, J. & Amir, A. Distinguishing different modes of growth using single-cell data. *eLife* **10**, e72565 (2021).
68. Govers, S. K., Campos, M., Tyagi, B., Laloux, G. & Jacobs-Wagner, C. Apparent simplicity and emergent robustness in the control of the *Escherichia coli* cell cycle. *Cell Syst.* **15**, 19–36 (2024).
69. Bailey, M. W., Bissichia, P., Warren, B. T., Sherratt, D. J. & Männik, J. Evidence for divisome localization mechanisms independent of the Min system and SlmA in *Escherichia coli*. *PLoS Genet.* **10**, 1004504 (2014).
70. Kar, P. Modeling analysis codes for: "Determining the rate-limiting processes for cell division in *Escherichia coli*" *Zenodo*, https://doi.org/10.5281/zenodo.13987797 (2024).

Acknowledgements

The authors thank Harold Erickson for valuable discussions, Scott Retterer for help in microfluidic chip making, and Joe Lutkenhaus and Sebastien Pichoff for plasmids. A part of this research was conducted at the Center for Nanophase Materials Sciences, which is sponsored at Oak Ridge National Laboratory by the Scientific User Facilities Division, Office of Basic Energy Sciences, U.S. Department of Energy. This work was supported by the National Institutes of Health award GM127413 (JM) and NSF MCB2313719 (JM). AA and PK acknowledge support from NSF CAREER 1752024. AA thanks for the generous support of the Clore Center for Biological Physics and ERC-CoG 2023 101125981.

Author contributions

JaanM and JaanaM designed the experiments, JaanaM contributed all the bacterial strains and plasmids and carried out the experiments, CA and JaanM designed, and CA fabricated the microfluidic devices, AA and PK developed the model and carried out modeling, JaanM wrote the manuscript. All authors commented on, edited, and approved the manuscript.

Competing interests

The authors declare no competing interest.

Additional information

Supplementary information The online version contains supplementary material available at https://doi.org/10.1038/s41467-024-54242-w.

Correspondence and requests for materials should be addressed to Jaan Männik.

Peer review information *Nature Communications* thanks Jodi Camberg and the other, anonymous, reviewers for their contribution to the peer review of this work. A peer review file is available.